Engineering Structures 293 (2023) 116596

Contents lists available at ScienceDirect

Engineering Structures

journal homepage: www.elsevier.com/locate/engstruct

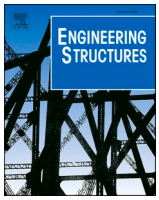

A new energy-dissipating RBS connection with double-nut-bolts: Seismic performance assessment and design methodology

Bahram Mirzaie Abar [a], Yashar Bakhshayesh [b], Reyes Garcia [c,*], Iman Hajirasouliha [d]

[a] Dept. of Civil Engineering, Faculty of Engineering and Technology, Imam Khomeini International University, Qazvin, Iran
[b] Dept. of Civil Engineering, Iran University of Science and Technology, Tehran, Iran
[c] Civil Engineering Stream, School of Engineering, The University of Warwick, Coventry, UK
[d] Dept. of Civil and Structural Engineering, The University of Sheffield, Sheffield, UK

ARTICLE INFO

Keywords:
Steel connections
RBS connections
Energy dissipating device
Design methodology
Finite element analysis

ABSTRACT

This article investigates analytically the seismic performance of a new RBS beam-column connection system with Double Nut Bolts (RBS-DNB) and double shear tabs. The bolts in the proposed RBS-DNB connection are used to: i) increase the strength of the beam's reduced section, ii) increase the energy dissipating capacity of the connection, and iii) delay damage of the beam in the plastic hinge zone. A reference RBS connection from the literature is first modeled and calibrated in Abaqus® software. A set of RBS-DNB connections are then designed (according to a new proposed method) and subsequently modeled in Abaqus®. The analytical results from the reference RBS connection and RBS-DNB connections are then compared in terms of cyclic response, beam strength, dissipated energy, beam hinge deformation and damage. The results show that, compared to the reference RBS connection, the proposed RBS-DNB connection system can increase the strength of the beam's reduced section and dissipate more energy by up to 16 % and 12 %, respectively. Moreover, a damage assessment shows that RBS-DNB connections can efficiently delay the initiation of beam hinging, and reduce buckling deformation and damage to the beam hinge compared to the reference RBS connection. The new proposed design method ensured the safe load-carrying mechanism of RBS-DNB connections, and it also predicted well the potential damage at the components of the RBS-DNB connections. Finally, the results of pushover analyses on typical 4-storey buildings with RBS-DNB connections demonstrated their higher lateral load bearing capacity compared to those with conventional RBS connections. This study contributes towards developing more robust energy-dissipating connections for steel buildings located in seismic areas.

1. Introduction

The failure of numerous beam-to-column connections of steel buildings damaged in past earthquakes (e.g. 1994 Northridge, 1995 Kobe, 2017 Sarpol-e Zahab Iran) has highlighted the need to reassess the design and construction practices of such critical components. In the last years, extensive experimental and numerical studies have been conducted aiming to: (1) retrofit inadequate pre-Northridge connections e.g. [1–3], (2) improve the design of steel structures [4,5], (3) introduce new improved bolted or welded connections [6–8], and (4) ensure a safe load-carrying capacity of connections [9–11]. The above advancements led to the prequalified beam-to-column connections included in current design guidelines [12]. Among the different prequalified connections, Reduced Beam Section (RBS) connections (see Fig. 1) are widely used in the construction of Special Moment Frames (SMFs) in seismic regions [13]. In RBS connections, part of the beam flanges (or beam web) is removed to concentrate the yielding demand at that location, which in turn keeps the plastic hinge away from the welded joint. The yielding and plastic deformation at the reduced beam section (which effectively acts as a "fuse") leads to a ductile failure of the connection due to beam hinging.

Past studies [14,15,16] examined numerically and experimentally the effect of the radius cut (Fig. 1(a)) on the behaviour of RBS connections. The results showed that the cuts in the beam flanges could promote plastic hinge formations and therefore help the RBS connection to effectively work as a structural fuse. However, significant plastic deformation and damage could occur along the inner edge of the radius cut towards the face of the column, leading to premature failure modes.

* Corresponding author.
E-mail address: reyes.garcia@warwick.ac.uk (R. Garcia).

https://doi.org/10.1016/j.engstruct.2023.116596
Received 8 March 2023; Received in revised form 15 June 2023; Accepted 9 July 2023
Available online 18 July 2023

In a study by Horton et al. [17], deep learning neural networks were developed to simulate the complex cyclic hysteresis behaviour of RBS connections and to predict their dominant failure mode. The effects of variable cuts [18] and straight cuts [19] in the beam flanges on the structural performance of RBS connections were also investigated (see Fig. 1(b) and (c), respectively). The results of these studies indicated that whilst RBS connections with tapered and straight cut beams met the limit states of connection strength, high stress concentrations occurred at the edges of the cuts.

As another alternative solution, Tsavdaridis et al. [20] performed finite element (FE) analyses on Reduced Web Section (RWS) connections (Fig. 1(d)) to show that a web opening could also led to a suitable performance and lower stress concentrations at the reduced section. Atashzaban et al. [21] also investigated analytically the performance of drilled flange (DF) RBS connections (Fig. 1(e)). The results showed that, as intended, the plastic strains and brittle fracture shifted from the Complete Joint Penetration (CJP) weld to the drilled flange holes. In order to minimize local buckling at the reduced section of the beam and improve its stability, Wu et al. [22] proposed fitting a restraining device around the RBS zone (Fig. 1(f)). However, severe buckling at the beam flange end still occurred, and the CJP welds failed in a brittle way.

Previous studies [18,23] have shown that tensile rupture of the reduced beam flange was the most common failure observed in RBS connections. Whilst adding restraining devices to the (weak) reduced beam section is a logical choice to delay failures in RBS connections, this option has not been thoroughly explored in the existing literature. Moreover, such restraining devices could also be used to increase the beam's strength at the reduced beam section, and to increase the stability after beam hinging occurs. The increment of the beam's strength would be particularly appealing to retrofit Pre-Northridge steel structures [1]. Indeed, when RBS connections are used to retrofit existing Pre-Northridge connections, the beam's strength is reduced due to the removal (cutting) of the flanges. Therefore, the reduced section of the beam could be strengthened with restraining devices to recover the original beam's strength. In summary, restraining devices in RBS connections can be used to: 1) enhance the beam's strength, 2) stabilize the reduced area of the beam, 3) delay damage and rupture at the beam cut, and 4) retrofit pre-Northridge connections using RBS. However, more studies are required to investigate to what extent the addition of restraining devices can improve the behavior of RBS connections.

To address some of the above-mentioned shortcomings of typical RBS connections, this article investigates analytically the behavior of a new type of RBS connection with Double-Nut-Bolts (RBS-DNB) and double shear tabs. After showing the details of the proposed RBS-DNB connection, a practical design methodology is presented for the new connection system. Next, a reference RBS connection is modeled and calibrated in Abaqus® software. A series of RBS-DNB connections are subsequently designed (following the proposed methodology) and modeled in Abaqus®. The numerical results from the reference RBS connection and RBS-DNB connections are then compared in terms of cyclic response, beam strength, energy dissipation and beam hinge deformation. A detailed damage assessment of critical components (beam hinge, beam flange, double nut bolts, CJP welds and shear tabs) is also performed. Finally, the structural response of SMFs with the new type of RBS-DNB connections is investigated using a pushover analysis. The results from this study contribute towards developing more robust energy-dissipating connections for steel buildings located in seismic areas.

2. Characteristics of the proposed RBS-DNB connection

Fig. 2(a) shows schematically the new proposed RBS-DNB connection. The four horizontal bolts placed at the sides of the RBS help to i) dissipate energy, ii) increase the beam strength at the reduced beam section, and iii) reduce lateral movements of the beam flange at large plastic deformations. Double nuts are also used to ensure the bolts can work both in tension and compression. The bolts are connected to internal stiffeners, which in turn are welded to the beam's flange and web. The stiffeners stabilize the section and minimize buckling around the RBS. In addition, double shear tabs are used to enhance the connection

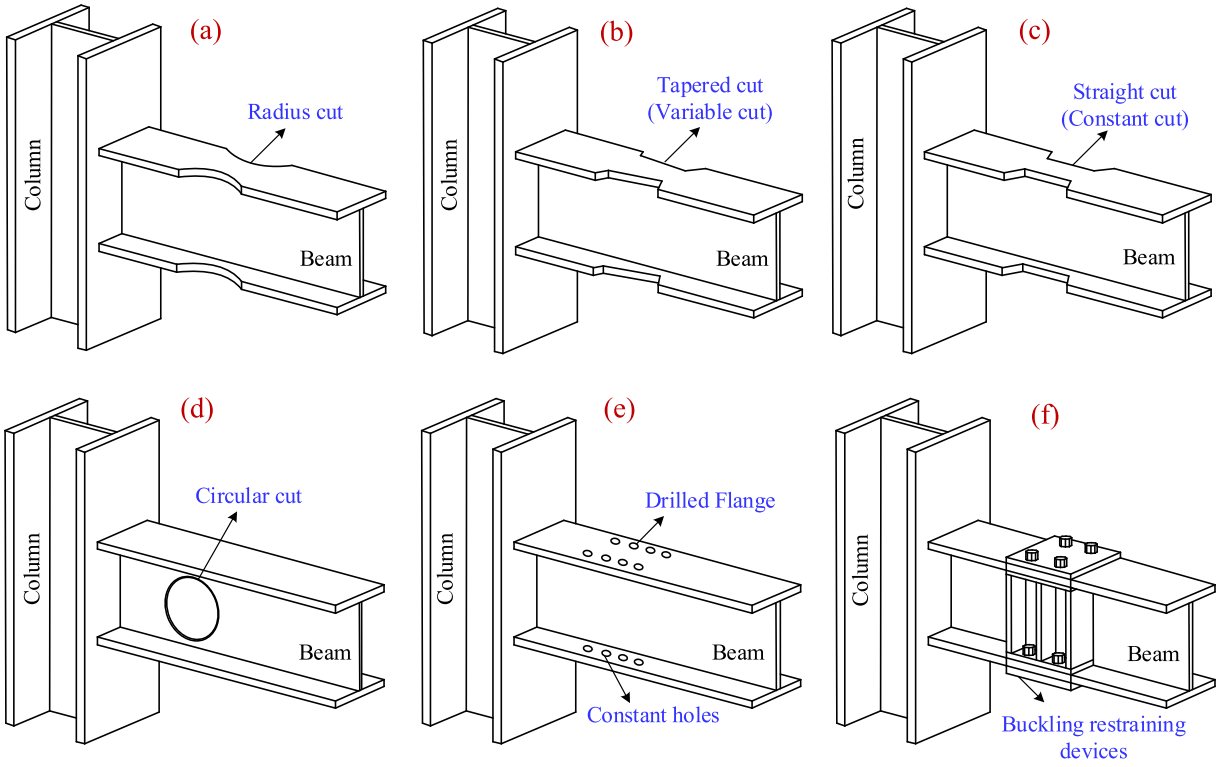

Fig. 1. Typical configurations of RBS connections: (a) radius cut [14–16], (b) tapered cut [18], (c) straight cut [19], (d) web circular cut [20], (e) drilled flange [21], and (f) buckling restrained devices [22].

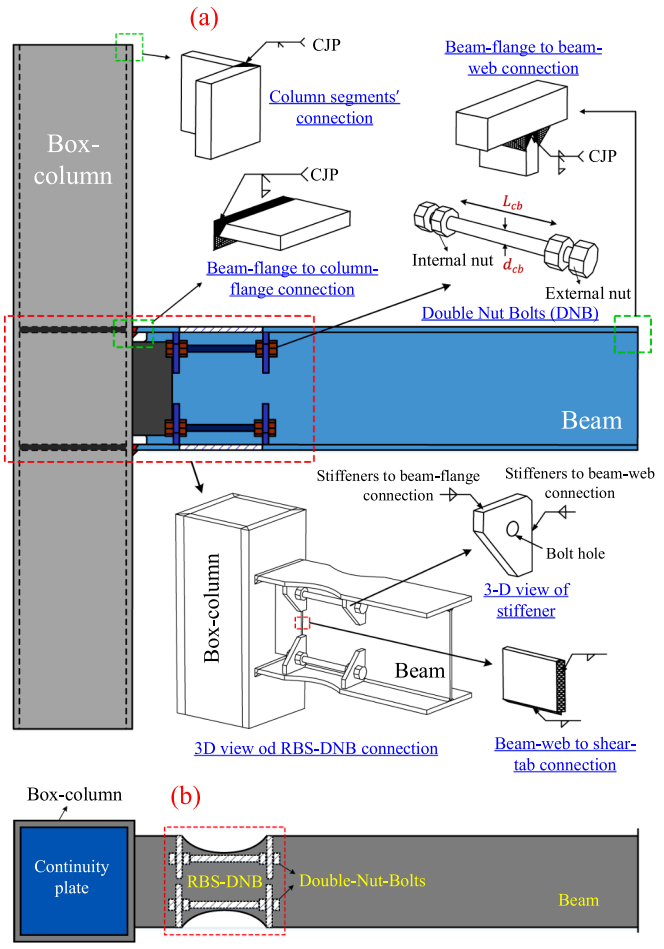

Fig. 2. Proposed RBS-DNB moment connection system: (a) fabrication details and connection components, and (b) top view of the RBS-DNB connection.

strength along the inner edge of the radius cut near the column face.

Fig. 2(a) also illustrates the fabrication details of the proposed RBS-DNB connection, including the internal stiffeners and double nut bolts. CJP welds are used to connect the beam flanges to the beam web (built-up beam), and to connect the column flanges to the column webs (built-up box column). Also, back welds are used at the beam-flange and the beam-web connection. Double shear tabs are connected to the beam web with fillet welds, and to the column using CJP welds. CJP welds are used to ensure a safe load-carrying mechanism from the beam flange to the column [9], and the corresponding root is back-welded. Double-sided fillet welds connect the internal stiffeners to the beam-flanges and to the beam-web to prevent stress concentrations and a potential tensile rupture of the beam's flanges and web.

In actual construction practice, the internal nuts of the new RBS-DNB (see Fig. 2(a)) would need to be tightened first. Next, pre-tensioning forces would be applied to the bolts to pre-load them internally. The external nuts would then be tightened and pre-tensioned to pre-load the bolts externally (i.e. the area of the bolts along the double nuts is pre-tensioned). In this way, the double nut bolts can transfer both tensile and compressive forces along the clear distance L_{cb} between internal nuts. The compressive (or tensile) strength of the bolts can be calculated using the bolt diameter d_{cb}, as shown later.

It should be noted that, in typical RBS connections, the cuts at the beam flanges reduce the effective width of the flange. This implies that part of the steel material in the flange (near its edges) is not fully utilized. In contrast, the proposed RBS-DNB connection uses the double-nut-bolts to recover part of the flexural strength lost by the removal of the cuts (potentially close to the strength provided by the full width of the beam flange), thus increasing the beam's utilizable cross sectional area (see Fig. 2(b)). This is shown in the design example presented in a subsequent section.

3. Proposed design methodology

Fig. 3 shows the parameters needed to design the RBS-DNB connection, including the geometry, load transferring mechanism and design forces, as well as details of the reduced beam section (view B-B) and internal stiffeners. In Fig. 3, the landing of the internal stiffeners (25 mm) and the bolt hole diameter (d_{cb} + 2 mm) are determined based on the AISC *Prequalified Connections* [12] and AISC *Specifications* [24] documents, respectively. The dimensions a_s and b_s of the internal stiffeners can be determined using the diameter of the nuts, as well as the size of the fillet welds of stiffener-to-beam and beam-flange to beam-web connections. For practical purposes, the stiffener height is taken as $\frac{d_b}{3}$, where d_b is the beam depth. The stiffener width is also considered as half of the beam flange width minus the web thickness (t_{bw}) and minus the fillet weld size (along the beam-flange to beam-web connection).

The flowchart shown in Fig. 4 summarizes the iterative design procedure of the proposed RBS-DNB connection, according to the following steps.

Step 1. A bolt diameter d_{cb} is initially chosen based on the beam depth: (i) for beam depths up to 350 mm, d_{cb} is suggested to be between 10 and 16 mm; and (ii) for beam depths bigger than 350 mm, choose greater than $18d_{cb}$ mm.

Step 2. Previous studies indicated that the tensile strength of double nut bolts is higher than their compressive strength [24,25]. Accordingly, the compressive strength of the bolts $F_{n,b}$ (refer to Fig. 5(b)) can be calculated using Eq. (1):

$$F_{n,b} = \varphi_c F_{cr} A_{cb} \tag{1}$$

where φ_c is a resistance factor for compression; F_{cr} is the flexural buckling stress of the bolt (considering the cross section and length of the bolt); and A_{cb} is the cross-sectional area of the bolt.

The value F_{cr} can be obtained from Eq. (2-a) or Eq. (2-b):

$$\text{if}: \ \frac{F_{y,bolt}}{F_e} \le 2.25 \rightarrow F_{cr} = \left(0.658^{\frac{F_{y,bolt}}{F_e}}\right) F_{y,bolt} \tag{2-a}$$

$$\text{otherwise}: \ \frac{F_{y,bolt}}{F_e} > 2.25 \rightarrow F_{cr} = 0.877 F_e \tag{2-b}$$

where $F_{y,bolt}$ is the minimum yield stress of the material used in the bolt; and F_e is the elastic buckling stress of the bolt. The value F_e is calculated using Eqs. (2-c)–(2-e).

$$F_e = \frac{\pi^2 E}{\left(\frac{L_c}{r}\right)^2} \tag{2-c}$$

$$L_c = 0.65 L_{cb} \tag{2-d}$$

$$r = \frac{d_{cb}}{4} \tag{2-e}$$

where E is the Young's modulus of steel; L_c is the effective length of the bolts [12]; L_{cb} is the distance of the internal edges of the internal nuts (Fig. 5(b)); and r is the radius of gyration of the bolt.

Step 3. The plastic moment of the beam ($M_{pr,b}$) and corresponding shear force ($V_{pr,b}$) at the center of the bolts and reduced beam section are calculated using Eq. (3) and Eq. (4), respectively. Likewise, and by considering the strength of the bolts, the design moment ($M_{ud,a}$) of the connection at the column face (see Fig. 3) is calculated using Eq. (5):

$$M_{pr,b} = C_{pr} R_y F_y Z_{RBS} + 4 F_{n,b} h_b \tag{3}$$

$$V_{pr,b} = \frac{2 M_{pr,b}}{L_0 - (2a + b)} \tag{4}$$

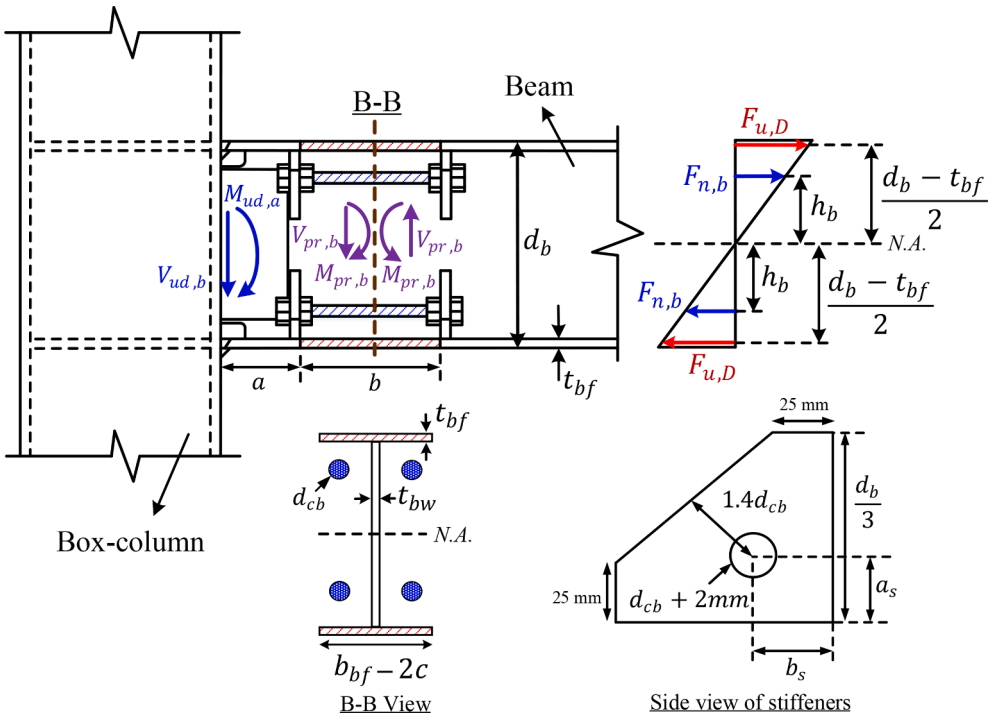

Fig. 3. Parameters needed to design RBS-DNB connection, including transferring mechanism of load demand and details of the reduced beam section (view B-B) and internal stiffeners.

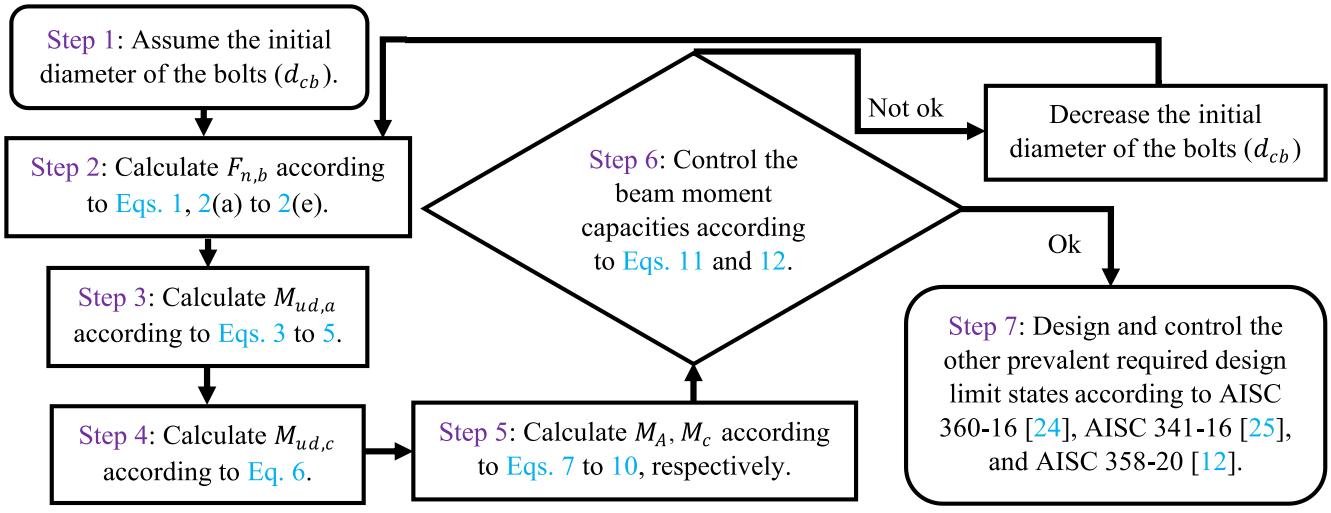

Fig. 4. Design flowchart of the proposed RBS-DNB connection system.

$$M_{ud,a} = M_{pr,b} + V_{pr,b}\left(a + \frac{b}{2}\right) \tag{5}$$

where the coefficient C_{pr} accounts for the peak connection strength (including connection conditions);R_y is the ratio of expected yield stress to the specified yield stress of the beam; F_y is the minimum yield stress of the beam's material; Z_{RBS} is the plastic section modulus of the reduced beam section;$F_{n,b}$ is the minimum value of the tensile or compressive strength of the bolts; h_b is the distance of the bolt's central axis to the (elastic) neutral axis of the beam; L_0 is the connected beam length;a is the horizontal distance of inner radius cut to the column face; and b is the radius cut length.

Step 4. Fig. 6 shows the moment demand diagram of the beam, assuming that the RBS-DNB connection can reach its ultimate design moment $M_{ud,a}$. Based on the design assumptions outlined above, the critical zones of the connection are: i) section A–A due to the large ultimate design moment at the column face and to the potential of a tensile rupture of the beams's flanges, shear tabs, and CJP welds, and ii) section C–C due to the beam's buckling deformation. The moment demand at section C–C corresponding to the moment demand diagram (Fig. 6) is obtained according to Eq. (6).

$$M_{ud,c} = M_{ud,a} \bullet \frac{2L_{lb}}{L_0} \tag{6}$$

where L_{lb} is the distance of the beam end to section C–C, while the other variables are as defined before.

Step 5. The calculated moment demand of the beam (Eqs. (5) and (6)) at the critical sections (Fig. 6) must be lower than the corresponding beam moment capacities. The beam moment capacities (Fig. 5(a)) at sections A–A (M_A) and C–C (M_C) are obtained using Eq. (7) and Eq. (8), respectively.

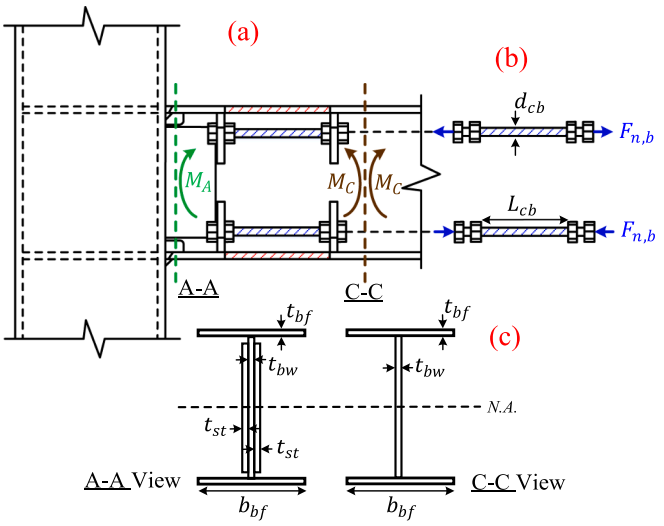

Fig. 5. RBS-DNB moment connection: (a) moment capacities of beam, (b) capacity of double nut bolts, and (c) dimensions of the beam section.

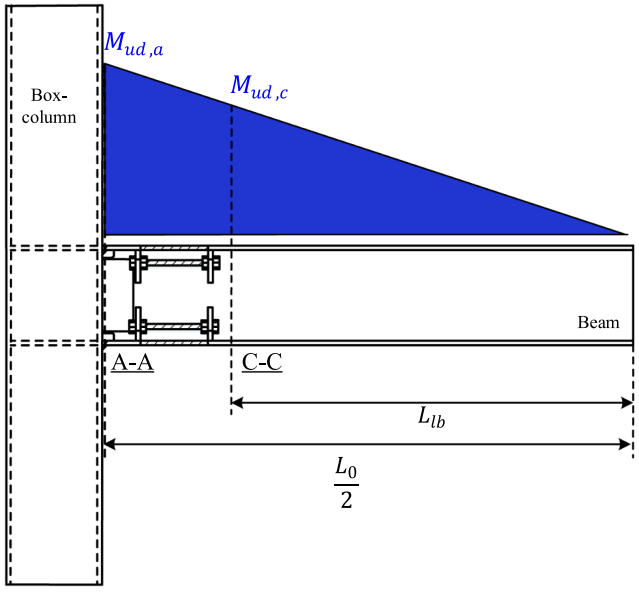

Fig. 6. Moment demand diagram of the connected beam based on the plastic moment of the beam hinge.

$$M_A = \varphi_d Z_A R_y F_y \tag{7}$$

$$M_C = \varphi_n Z_C R_y F_y \tag{8}$$

where φ_d and φ_n are the resistance factors for ductile and non-ductile limit states, respectively. Z_A and Z_C are the plastic section moduli of the beam at sections A–A and C–C, respectively (see Fig. 5(c)).

The moduli Z_A and Z_C can be calculated based on Eq. (9) and Eq. (10), respectively:

$$Z_A = 2b_{bf}t_{bf}\left(\frac{d_b - t_{bf}}{2}\right) + \frac{t_{st}}{2}(d_b - 2t_{bf} - 2h_{a,c})^2 + \frac{t_{bw}}{4}(d_b - 2t_{bf} - 2h_{a,c})^2 \tag{9}$$

$$Z_C = 2b_{bf}t_{bf}\left(\frac{d_b - t_{bf}}{2}\right) + t_{bw}\left(\frac{d_b - 2t_{bf}}{4}\right)^2 \tag{10}$$

where b_{bf} is the width of the beam flange and $h_{a,c}$ is the height of the access holes of the beam web.

Step 6. Eq. (11) and Eq. (12) should be satisfied to ensure the utilized bolt's diameter leads to the moment demands that are slightly lower than the moment capacities. Otherwise, the whole design process should be repeated by using a smaller diameter d_{cb} (see flowchart in Fig. 4).

$$M_{ud,a} \le M_A \tag{11}$$

$$M_{ud,c} \le M_C \tag{12}$$

Step 7. To obtain the final design solution, other prevalent limit states applicable to RBS-DNB should also be checked in accordance with AISC *Prequalified Connections* [12], AISC *Seismic Provisions* [25] and AISC *Specifications* [24].

4. Numerical investigation

The numerical investigation is divided into two parts:

- A reference full-scale RBS connection tested by [26] was modeled and calibrated in Abaqus® software [27].
- A series of RBS-DNB connections were designed following the design procedure in Section 3. The connections were subsequently modeled in Abaqus® to assess the effect of key design parameters on the structural behavior of the proposed systems.

4.1. FE modeling and calibration of RBS connection

FE modeling. The reference RBS connection in [26] was designed according to the AISC *Prequalified Connections* [12]. The beam had a radius cut with the dimensions shown in Fig. 7(a). The Abaqus® model included the beam and box-column elements, as well as the lateral support conditions shown in Fig. 7(a). Table 1 summarizes the material properties of the beam and column sections of the reference RBS connection. The double nut bolts were assumed to be of A490 steel. The bolts were preloaded according to AISC 360 [24] with loads of 45 kN for the M10 bolts, 64 kN for the M12 bolts, 87 kN for the M14 bolts, 114 kN for the M16 bolts, 144 kN for the M18 bolts, and 179 kN for the M20 bolts. A slip coefficient of 0.3 between the steel plates and bolts was assumed, according to the recommendations in AISC 360 [24] and AISC 358 [12]. The steel material was modeled using a von-Mises yield criterion and an isotropic-hardening plastic behavior, with a Young's modulus of 210 GPa, a Poisson's ratio of 0.3, and true stress–strain relations [27]. It should be noted that true stress–strain relations were used instead of the engineering stress–strain from coupon tests, according to recommendations from previous research [9] Fig. 8(a)–(c) show, respectively, the stress–strain relationships adopted in the modeling of beam, column and bolts. To consider the buckling deformation of the beam section (including the radius cut and double nut bolts), large strains and deformations were defined as geometry nonlinearities. Tie contact was used to connect the connection components as recommended in [9,11,28,30]. The boundary conditions were defined based on the support conditions shown in Fig. 7(a). Fig. 7(b) shows the adopted loading protocol (as story drift angle) applied to the beam tip [25,26,29]. Likewise, Fig. 7(c) shows the constraint conditions adopted in the FE modeling. Pinned boundary conditions (i.e. $X = Y = Z = 0$ based on general coordinates) were considered at the top and bottom of the column. The displacement-controlled loading protocol was applied at the tip of the beam in the Y-direction (i.e. $Y = -1$). The beam was laterally supported (i.e. $Z = 0$) to prevent out-of-plane movement, but the beam was free to move in the X-direction [9]. A general static step was considered in the analysis as a direct equation solver based on the solution technique of the full Newton-Raphson method [27].

The meshed model of the reference RBS connection and its key components are shown in Fig. 9. Sweep elements were used to mesh the CJP and fillet welds, whereas structured elements were used to mesh the column, beam, and continuity plates to have a regular mesh. 8-node linear brick elements (Solid 3D C3D8R) with reduced integration were

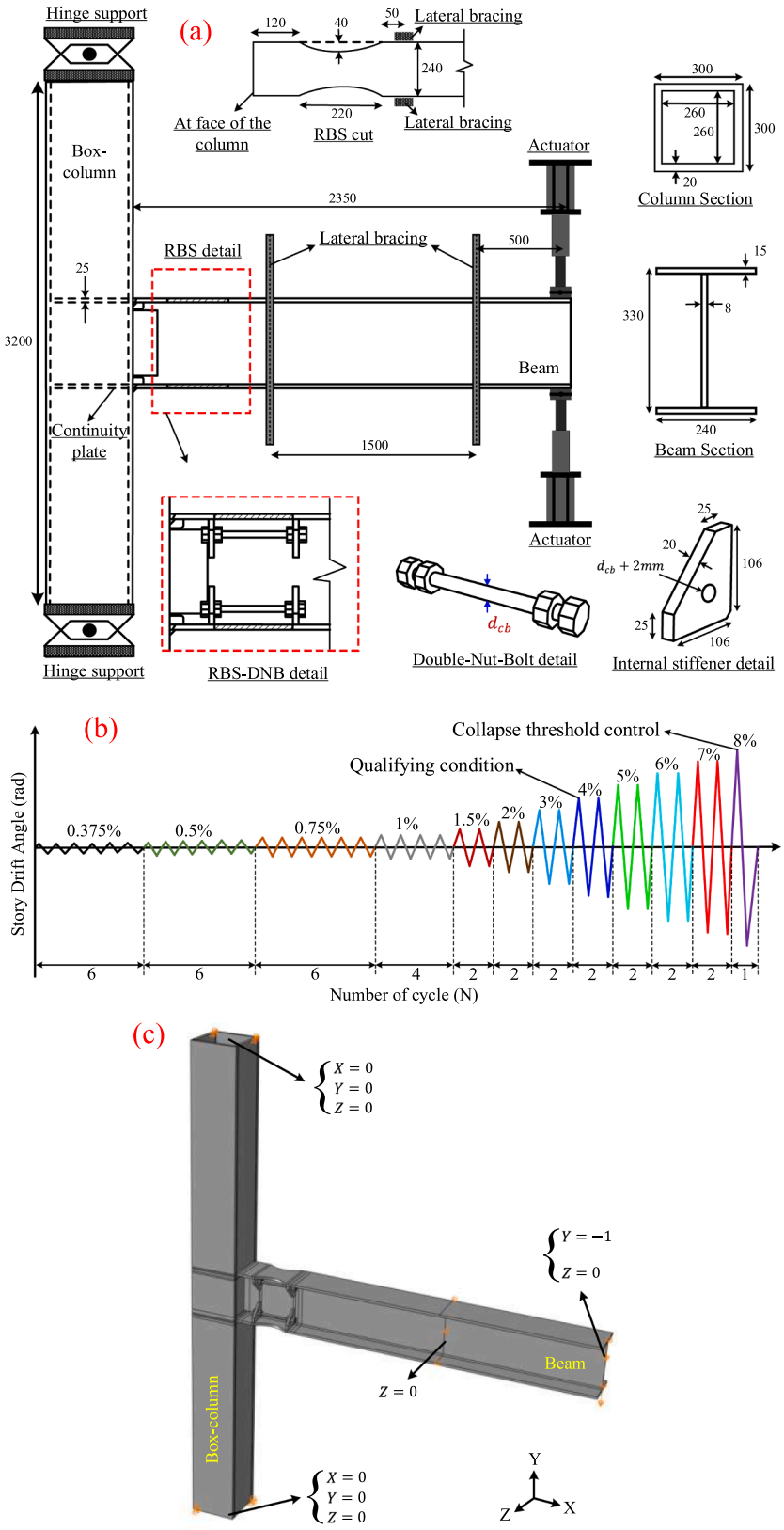

Fig. 7. Reference RBS connection modeled in Abaqus®: (a) geometry and test setup [26], (b) loading protocol [25,26], and (c) constraint conditions of FE models (units: mm).

Table 1
Material properties of components of RBS and RBS-DNB connections (units: MPa).

ID	Beam			Column			A490 double nut bolts		
	$F_{y,b}$	$F_{u,b}$	$\varepsilon_{u,b}$(%)	$F_{y,c}$	$F_{u,c}$	$\varepsilon_{u,c}$(%)	$F_{y,bolt}$	$F_{u,bolt}$	$\varepsilon_{u,bolt}$(%)
RBS [26]	261	397	35	273	431	20	–	–	–
RBS-DNB	261	397	35	273	431	20	900	1000	14

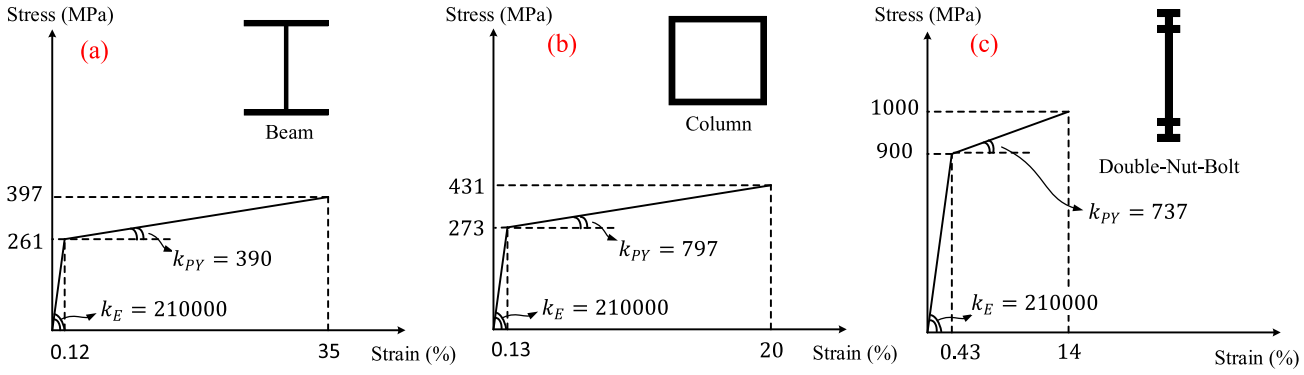

Fig. 8. Schematic stress–strain relationships of steel materials used in (a) beam, (b) column, and (c) bolts (not to scale).

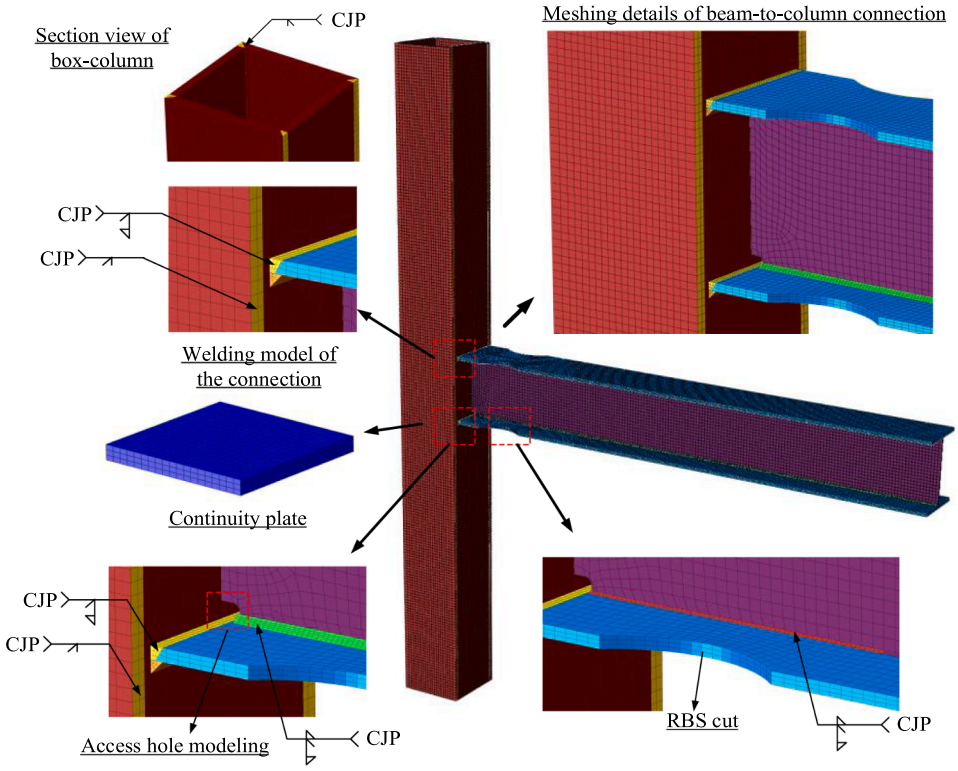

Fig. 9. Meshed model and welding details of the RBS connection.

used to model the deformable components to capture accurately their stress conditions. An hourglass control [27] was used to prevent analysis terminations due to element distortion, element separation and/or element penetration. A mesh sensitivity analysis was performed to determine the required mesh size. It was found that values of ~83000 elements and ~111000 nodes resulted in the best agreement between the numerical and experimental results with reasonable computational costs. As the number of elements and nodes increased beyond such values, the numerical results remained practically unchanged. An elastic buckling analysis was also performed to capture the value of the first eigenmode, which was imposed to the developed FE model to simulate the initial imperfections of the reference RBS connection tested in [26].

Calibration of model results. Fig. 10(a) and (b) compare the beam hinge deformation and equivalent plastic strain (PEEQ) distribution obtained from Abaqus® with the corresponding results from the experiments at drift ratios of 4.0 % and 7.0 %, respectively. The results show that the experimental beam buckling deformation and PEEQ were well predicted by the developed numerical model. Fig. 10(c) also shows

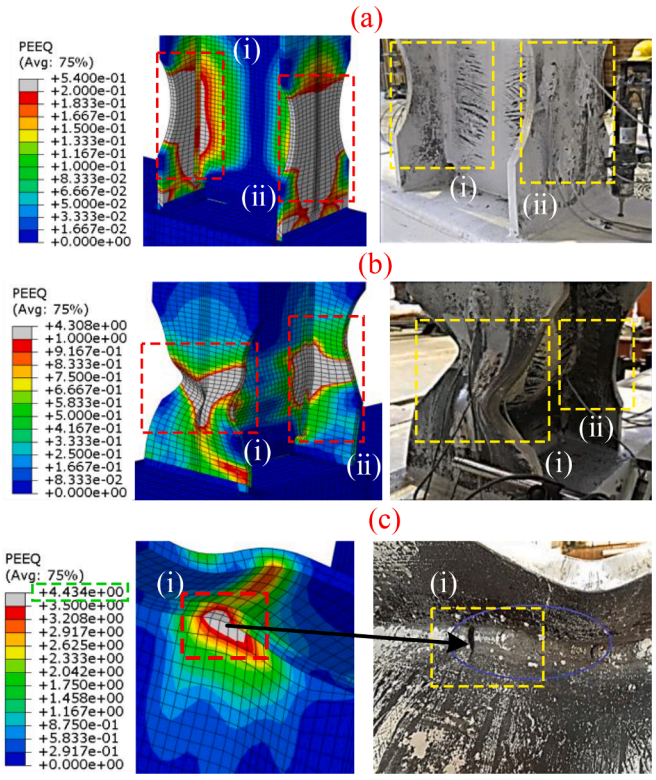

Fig. 10. Comparison of beam hinge deformation and PEEQ distribution from Abaqus® and from experiment on RBS connection at (a) 4.0 % drift ratio, (b) 7.0 % drift ratio, and (c) weld rupture.

that the model captured well the damage in the beam at failure, which was dominated by weld rupture. The benchmark value of crack propagation and weld rupture based on the PEEQ counter was 4.43, as highlighted in green in Fig. 10(c).

Fig. 11(a) compares the experimental and numerical cyclic moment-drift responses of the reference RBS connection. It is shown that the Abaqus® model predictions agree very well with the measured experimental responses. This observation is confirmed by the skeleton curve shown in Fig. 11(b), where the calculated errors in each cycle are also included. Overall, the small errors (around 1.5 % average error in the positive and negative directions) confirm that the calibrated model captures accurately the behavior of the reference RBS connection.

4.2. Design and specifications of RBS-DNB connections

A series of nine RBS-DNB connections were designed in accordance with the design procedure presented in Section 3. The nine RBS-DNB connections had the same geometry and loading protocol (Fig. 7(b)) as the reference RBS connection. However, the stiffener and bolts of the RBS-DNB connections (Fig. 7(a)) were incorporated in the modeling. The material properties of the beam and box-column sections were also the same, as summarized in Table 1. Table 1 also shows the material properties of the high-strength A490 bolts that were assumed as Double Nut Bolts.

Table 2 lists the specifications of the RBS-DNB connections analyzed in this study. The ID of the connections include the bolt diameter in mm (e.g. M10 = 10 mm). Note that some of the RBS-DNB connections in Table 2 had different bolt sizes at the top and bottom of the reduced beam section in order to assess their effect on improvements in the response. For instance, RBS-M16-M14 had bolts of 16 mm at the top and 14 mm at the bottom. Table 2 also summarizes the calculated moment demands ($M_{ud,a}$ and $M_{ud,c}$), moment capacities (M_A and M_C), and corresponding demand to capacity ratios at the critical A-A and C–C sections of the connections. Table 2 also provides the predicted failure mode of each connection based on the calculated demand to capacity ratios. In this study, connection RBS-M16 was deemed as the 'main' RBS-DNB connection (due to its demand to capacity ratios being just below or equal to 1.0), whereas other RBS-DNB connections with different bolt diameters (M10, M12, M14, M18 and M20) were considered as 'parametric' connections. Appendix A presents the full design of connection RBS-M16 according to the new method proposed in Section 3. It is worth noting that the use of different bolt sizes at the top and bottom of the beam shifted its neutral axis towards the larger bolts. This leads to larger design forces at a beam flange near the larger bolts, which in turn can cause damage to the CJP welds, shear tabs, or beam flange adjacent to the column face (see Table 2). The potential damage of these components will be evaluated in Section 5 of this article.

Fig. 12 compares the demand to capacity ratios at critical sections of the reference RBS and RBS-DNB connections. The parametric connections were divided into "lower bound" (with under strength bolts) and "upper bound" (with over strength bolts) to assess the efficiency and safety of the proposed design method in the following sections.

5. Comparison of results: RBS vs RBS-DNB connections

Beam strength. Fig. 13(a) to (i) compare the cyclic (numerical) responses of the reference RBS connection and RBS-DNB connections. These figures also show the strength enhancement in percentage, as well as the beam plastic moment (M_p = 343 × 10^6 N·mm) calculated as shown in Appendix A. The results indicate that all the studied RBS and RBS-DNB connections reached more than 80 % of their beam strength at 4.0 % drift ratio. Accordingly, all connections satisfied the AISC *Seismic Provisions* [25] and could be used in construction of Special Moment Frames (SMFs). In general, RBS-DNB connections had larger hysteresis loops and higher strengths than the reference RBS connection. For instance, connection RBS-M16 had around 16 % higher strength than the RBS connection. Likewise, the corresponding strengths of RBS-M18 (Fig. 13(e)) and RBS-M20 (Fig. 13(f)) increased by around 20 %

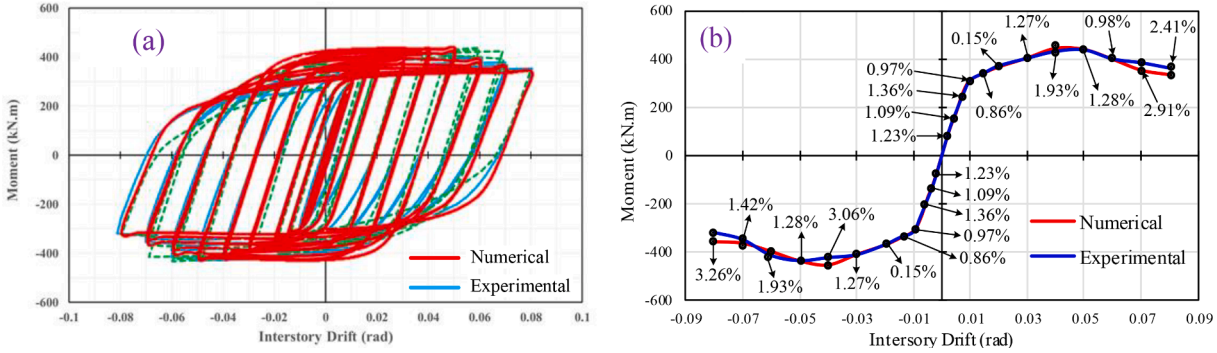

Fig. 11. Experimental and numerical moment-drift responses of RBS connection: (a) cyclic, and (b) skeleton curve.

Table 2
Design results of reference RBS connection and RBS-DNB connections (units: kN·m).

ID	Bolt diameter (d_{cb})	$M_{ud,a}$	$M_{ud,b}$	$M_{ud,c}$	M_A	M_C	$\frac{M_{ud,a}}{M_A}$	$\frac{M_{ud,c}}{M_C}$	Predicted failure mode
RBS [26]	–	337.11	304.16	286.90	337.73	308.65	0.99	0.93	Beam hinge
RBS-M10	M10	332.72	306.68	283.16	367.89	308.65	0.90	0.92	Beam hinge Bolts
RBS-M12	M12	343.02	309.45	291.93	367.89	308.65	0.93	0.94	Beam hinge Bolts
RBS-M14	M14	348.07	314.01	296.23	367.89	308.65	0.95	0.96	Beam hinge Bolts
RBS-M16	M16	355.92	321.09	302.91	367.89	308.65	1.00	0.98	Beam hinge Bolts
RBS-M18	M18	366.24	330.40	311.70	367.89	308.65	1.00	1.01	Beam flange CJP welds
RBS-M20	M20	373.11	336.61	317.54	367.89	308.65	1.02	1.03	Beam flange CJP welds Shear tabs
RBS-M16-M14	Top-M16 and bottom-M14	352.14	317.69	299.96	367.89	308.65	0.96	0.97	Beam flange Bolts
RBS-M18-M16	Top-M18 and bottom-M16	360.79	325.98	307.47	367.89	308.65	0.98	1.00	Beam flange CJP welds Shear tabs
RBS-M20-M18	Top-M20 and bottom-M18	369.91	333.53	314.83	367.89	308.65	1.01	1.02	Beam flange CJP welds Shear tabs

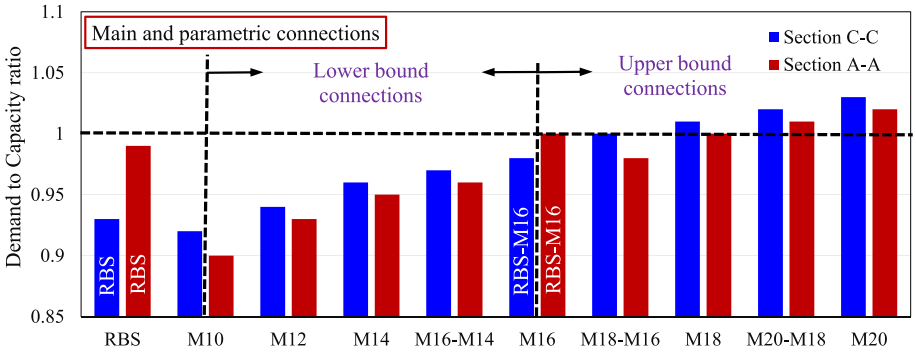

Fig. 12. Demand to capacity ratios at critical sections A-A and C–C.

compared to the reference RBS connection, although both RBS-M18 and RBS-M20 exhibited unacceptable demand to capacity ratios (see Table 2). The use of different bolt sizes at top and bottom of the beam (Fig. 13(g)–(i)) resulted in 13.5 %, 19.5 %, and 21.0 % higher beam strength in RBS-M16-M14, RBS-M18-M16, and RBS-M20-M18 connections compared to the RBS connection, respectively (see also M/M_p in Table 3). The effect of using different bolt sizes on the extent of damage to the beam flange, CJP weld, and shear tabs (see the last column of Table 2) are discussed in Section 6. Overall, the results confirm that the use of double nut bolts were very effective at enhancing the strength of the RBS-DNB connections.

Energy dissipation. Table 3 also lists the energy dissipated by the connections, which was calculated as the area inside the hysteresis loops up to a story drift of 8.0 % (see Fig. 13(a) to Fig. 13(i)). This parameter is especially important to assess the seismic performance of the whole structural system, as high energy dissipation in the connection can lead to lower damage in other structural elements. It is shown that, compared to the reference RBS connection, RBS-M16 had around 12 % higher energy dissipation capacity at such 'collapse' drift. An increase in the bolt diameter also increased the energy dissipation (by up to 19 % for RBS-M20-M18).

Beam hinge buckling deformation and initiation of hinging. The buckling deformation of the beam hinge, which acts as fuse element, gives an indication of the seismic performance of RBS connections. However, excessive buckling deformations can lead to premature beam failure at the fuse zone [26], and hence buckling deformations should be controlled to ensure a safe load-carrying mechanism in the connection. Table 3 compares the maximum buckling deformation of the connections. The results show that whilst the RBS connection had a buckling deformation of 56.3 mm, RBS-M16 had a buckling deformation of 40.5 mm (i.e. around 28 % lower). In all cases, the use of bolts limited the beam hinge deformation and improved the performance of RBS-DNB connections. Moreover, an increase in the bolt size reduced further the buckling deformation at the beam hinge. The results in Table 3 also indicate that, in all RBS-DNB connections, beam hinging initiated later than in the RBS connection. Therefore, the bolts could delay the beam hinge initiation, thus leading to a better performance of all RBS-DNB connections. It is worth noting that the flexural strength recovered by the double nut bolts was 18.9 % in connection RBS-M16 (see last substep in Appendix A), thus showing that the double nut bolts can recover some of the flexural strength lost by the removal of the cuts in RBS-DNB connections.

It should be mentioned that even if the cyclic response and buckling deformations of RBS-DNB connections are satisfactory, this type of connections may still experience excessive damage and premature failure at different locations. Therefore, the following sections compare the performance of RBS and RBS-DNB connections by assessing the failure modes of the beam hinge and bolt, as well as the damage of the beam flanges, shear tabs, and CJP welds of the connections' components. This assessment is necessary to ensure the safe load-carrying mechanism of the connections, and to assess the efficiency of the proposed design method to provide RBS-DNB connections with satisfactory performance.

6. Damage assessment and failure modes

6.1. PEEQ at beam hinge and plastic strains in bolts

The results presented in Fig. 10(c) and Table 1 show that beam hinge failure of the benchmark RBS connection occurred at a PEEQ value of 4.4, while the ultimate strain of the double nut bolts was 14 %. Based on these observations, PEEQ values above 4.4 at the beam hinge location can be used to define the theoretical failure of RBS-DNB connection. The results of the validated analytical models also indicate that the potential (theoretical) failure of the bolts generally occurs at plastic strains above 15 % (see Fig. 14).

Fig. 14(a)–(i) compare the PEEQ distribution of the beam hinge zone

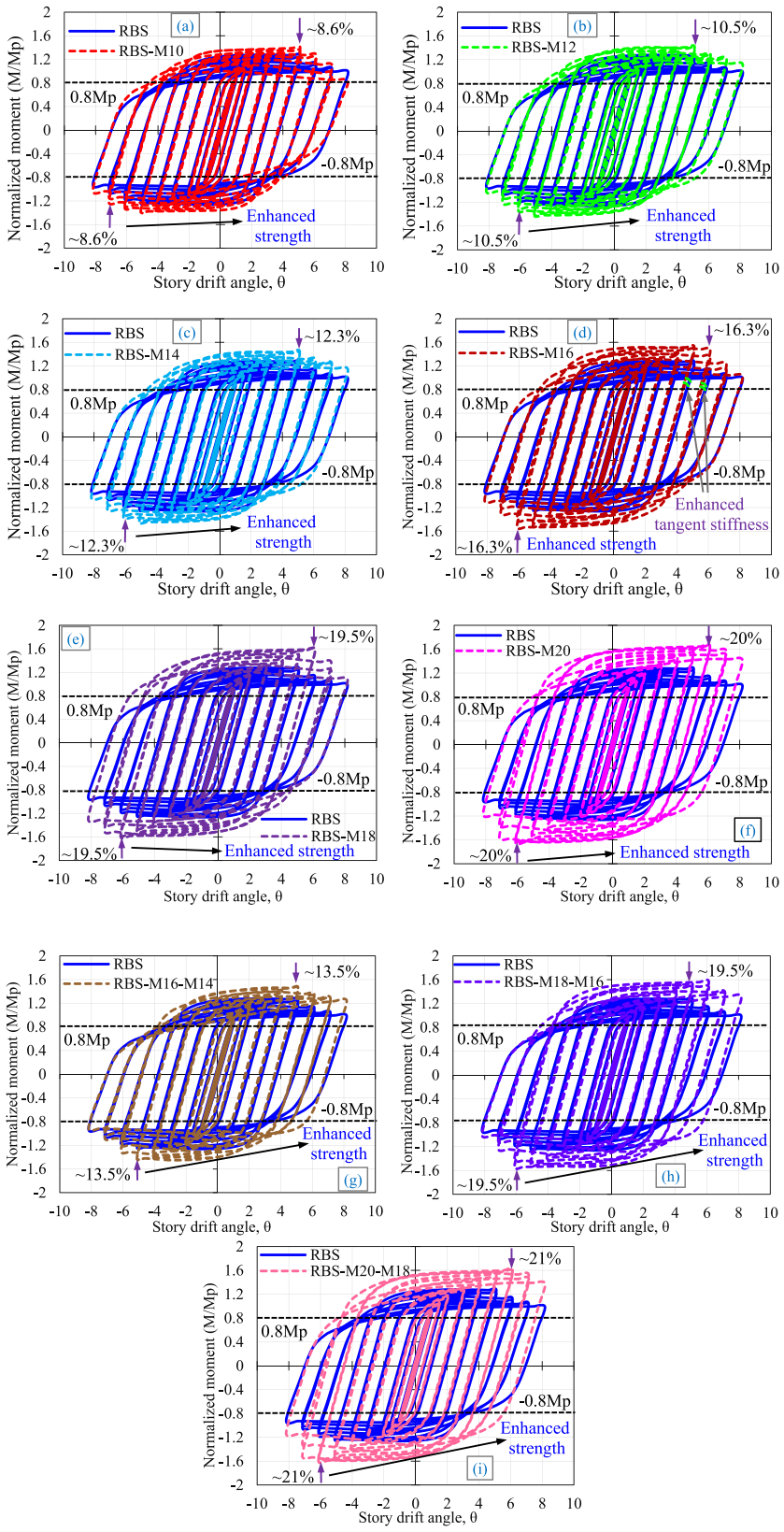

Fig. 13. Cyclic response of RBS and RBS-DNB connections: (a) RBS-M10, (b) RBS-M12, (c) RBS-M14, (d) RBS-M16, (e) RBS-M18, (f) RBS-M20, (g) RBS-M16-M14, (h) RBS-M18-M16, and (i) RBS-M20-M18.

Table 3
Comparison of Abaqus® results of RBS and RBS-DNB connections.

ID	$\frac{M}{M_p}$	Change (%)	Dissipated energy at drift = 8.0 % (kJ)	Change (%)	Beam hinge deformation (mm)	Change (%)	Beam hinge initiation	Change (%)
RBS [26]	1.28	–	510	–	56.3	–	4.5 %	–
RBS- M10	1.41	9.22%↑	550	7.8%↑	53.8	4.44%↓	5.0 %	11.1%↑
RBS-M12	1.43	10.49%↑	558	8.6%↑	40.1	28.77%↓	5.0 %	11.1%↑
RBS-M14	1.46	12.33%↑	572	10.8%↑	36.2	35.70%↓	5.1 %	13.3%↑
RBS-M16	1.53	16.34%↑	579	11.9%↑	40.5	28.06%↓	5.9 %	31.1%↑
RBS-M18	1.59	19.50%↑	584	12.7%↑	42.5	24.51%↓	6.1 %	35.5%↑
RBS-M20	1.60	20.00%↑	590	13.6%↑	45.1	19.89%↓	7.0 %	55.5%↑
RBS-M16-M14	1.48	13.51%↑	612	16.7%↑	27.0	52.04%↓	5.0 %	11.1%↑
RBS-M18-M16	1.59	19.50%↑	620	17.7%↑	25.9	53.99%↓	6.0 %	33.3%↑
RBS-M20-M18	1.62	20.98%↑	631	19.2%↑	23.1	58.97%↓	6.3 %	40.0%↑

and the plastic strain (PE) distribution of the double nut bolts (red highlights) of the RBS-DNB connections obtained from the FE models. The results in Fig. 14(a)–(c) indicate that although the beam hinge of RBS-M10, RBS-M12 and RBS-M14 had PEEQ values are below 4.4, failure occurred at the bolts as the PE in the double nut bolts reached around 20 %. However, the double nut bolts reduced damage and delayed failure of the beam's plastic hinge in the connections. Fig. 14(d) shows that the maximum PEEQ value at the beam hinge of RBS-M16 was 3.9, i.e. 12 % lower than the corresponding value (4.4) of the reference RBS connection. The bolts of RBS-M16 reached a plastic strain of 15 %, which suggests that the bolts experienced severe damage (i.e. failure). The results in Fig. 14(g) and (h) indicate the use of different bolt sizes in connections RBS-M16-M14 and RBS-M18-M16 led to failure at the beam hinge, as indicated by PEEQ values of 7.3 and 5.0 respectively. Based on these observations, it is recommended to use the same size of bolts in RBS-DNB connections. This in turn can simplify the design and construction of RBS-DNB connections in practical applications.

Fig. 15(a) and (b) summarize the maximum PEEQ values at the beam plastic hinge and the maximum PE values of the bolts, respectively. For comparison purposes, the figures also show the PEEQ value (4.4) and ultimate strain of the bolts (14 %) of the reference RBS connection. The results in Fig. 15(a) and (b) confirm that the bolts of RBS-M16 and RBS-M18 experienced severe damage, but no beam hinge failure occurred. Fig. 15(b) also shows that the dominant failure mechanism in the 'lower bound' connections (RBS-M10, RBS-M12, RBS-M14) was due to failure of the bolts. On the other hand, in the connections with different bolt size (RBS-M18-M16 and RBS-M16-M14), both the beam hinge and the bolts failed. Whilst Fig. 15(a) and (b) show that connections RBS-M20 and RBS-M20-M18 did not fail at the beam plastic hinge nor at the bolts, they may still exhibit damage and failure at the connection components. These potential failures are evaluated in the following section.

6.2. Damage at CJP welds, beam flange, and shear tabs

According to the AISC *Prequalified Connections* [12], the beam-to-column connection components (beam flanges, CJP welds and shear tabs that connect the beam flanges and web to the column) should remain within the elastic range to ensure the safe load-carrying mechanism of a connection. To assess these aspects in the proposed RBS-DNB connections, the maximum PEEQ values at the edges of the CJP weld (critical points A and B in Fig. 16(a)), beam flange (critical points C and D in Fig. 16(b)), and shear tabs (critical point E in Fig. 16(c)) were obtained from the Abaqus® models of the connections.

Fig. 17(a)–(e) compare the maximum PEEQ values at the critical points A to E, correspondingly. The results indicate that connection RBS-M20 had a higher potential of damage at the CJP weld, beam flange, and shear tabs (up to 32 % at point A) compared to the reference RBS connection. This implies that RBS-M20 did not satisfy the AISC *Prequalified Connections* requirements [12], as predicted by the proposed RBS-DNB design method (Section 4.2; Table 2 and Fig. 12). The results in Fig. 17(a)–(e) also show that connections RBS-M18, RBS-M20, RBS-M20-M18 and RBS-M18-M16 experienced some damage at the CPJ weld, shear tabs, or at the beam flange. This confirms that the proposed design method for RBS-DNB connection (Section 3) could predict well the potential damage at the A-A critical section in all the above-mentioned connections. It should be noted that the use of different bolt sizes in these connections led to a shift of the beam neutral axis towards the larger bolt sizes, which resulted in a damage in the CJP weld and shear tabs, as correctly predicted before in Section 4.2 and Table 2.

Connection RBS-M20-M18 had a demand to capacity ratio of slightly above 1.0 (Table 2) in the beam flange zone. Fig. 17(c) shows that this connection experienced a 2 % potential of damage at point C, as correctly predicted by the proposed design method. Consequently, besides the high potential of damage to the CJP welds in connections RBS-M20 and RBS-M20-M18, the beam flanges and shear tabs also experienced some damage, which is considered to be an inadequate structural performance.

Table 4 summarizes the potential damage and/or failure of the RBS-DNB connections as predicted by the FE models. It is shown that connections RBS-M10, RBS-M12 and RBS-M14 experienced failure of the bolts, as correctly predicted by the proposed design method. Therefore, the RBS-DNB design method provided a suitable design in terms of preventing failure mechanism at sections A–A and C–C, instead promoting failure of the double nut bolts. Connections RBS-M20 and RBS-M20-M18 had a high potential of damage to the beam flanges, shear tabs, and CJP welds, whereas the CJP welds and shear tabs were also damaged in RBS-M18 and RBS-M18-M16 connections. The results indicate that the proposed design method successfully ensured the safe load-carrying mechanism of RBS-DNB connections. The use of variable bolt sizes in RBS-M18-M16 and RBS-M16-M14 resulted in a faster beam hinge failure than the RBS connection, which confirms that the use of different bolt sizes is not recommended. The RBS-M16 that was designed with the proposed RBS-DNB method had a high potential of damage at the bolts, but this was expected as the double nut bolts work as energy-dissipating devices leading to better overall structural performance.

7. Seismic behavior of buildings with RBS or RBS-DNB connections

7.1. Case study SMF building

To evaluate the effectiveness of RBS-DNB connections at improving the seismic performance of steel buildings, a typical 4-story 3-bay Special Moment Frame (SMF) (Fig. 18(a) and (b)) was modeled and analyzed in SAP2000® [33]. The residential building was assumed to be built in a high seismicity region according to the Iranian seismic code [31], considering a PGA = 0.35 g. The building was designed in

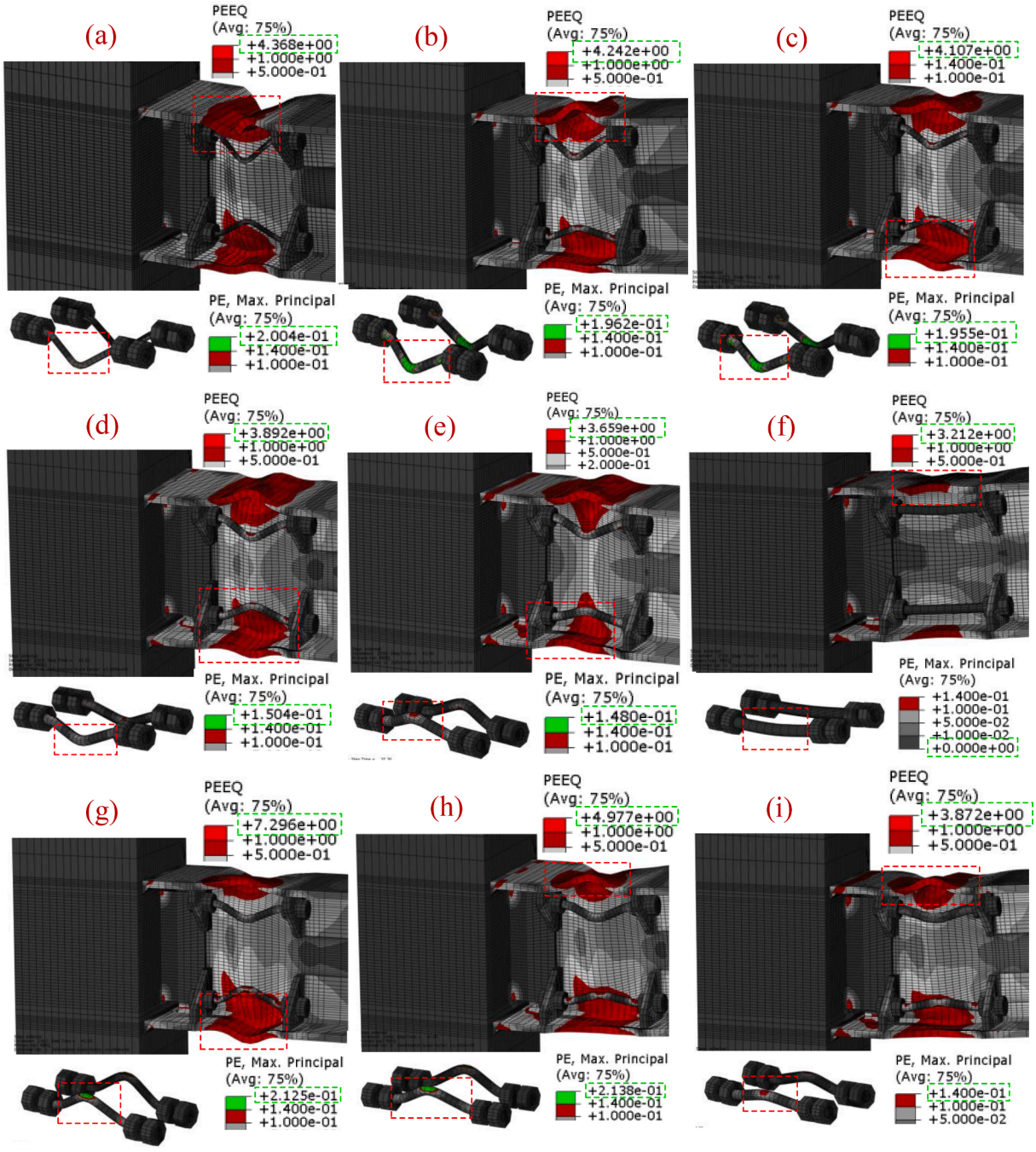

Fig. 14. PEEQ distribution in connections and PE distribution in bolts of RBS-DNB connections: (a) RBS-M10, (b) RBS-M12, (c) RBS-M14, (d) RBS-M16, (e) RBS-M18, (f) RBS-M20, (g) RBS-M16-M14, (h) RBS-M18-M16, and (i) RBS-M20-M18.

accordance with the AISC *Specifications* [24]. The dead and live loads of the stories were 5.0 kN/m^2 and 2.0 kN/m^2, respectively. The column height and bay length were 3.0 m and 5.0 m, respectively. The box column sections (see Fig. 18(b)) were 240 × 240 × 20 mm for the first and second floors, and 240 × 240 × 15 mm for the third and fourth floors. A similar I beam section was chosen for all stories, with a web of 300 × 8 mm and a flange of 240 × 15 mm. Note that the selected beam section was the same as the reference RBS connection [26] shown in Fig. 7(a).

7.2. Nonlinear pushover analysis

An intermediate frame of the building (red highlight in Fig. 18(a)) was selected to perform nonlinear pushover analyses. Two pushover load patterns (first mode and uniform pattern) were considered, according to ASCE41-06 guidelines [32]. Likewise, two gravity load combinations were adopted in the analyses: (i) a higher limit gravity load combination (GH) with 1.1 dead loads combined with 1.1 live loads, and (ii) a lower limit gravity load combination (GL) with a 0.9 dead load [32].

The nonlinear behavior of the members was modeled as concentrated plastic hinges at the ends of columns and beams, whereas the beam-to-column and column-to-column nodes were modeled as rigid nodes. The behavior of the P-M3 plastic hinges of columns was defined with the parameters given in ASCE41-06 tables [32]. The plastic hinges of beams were defined according to the reference RBS [26] and RBS-

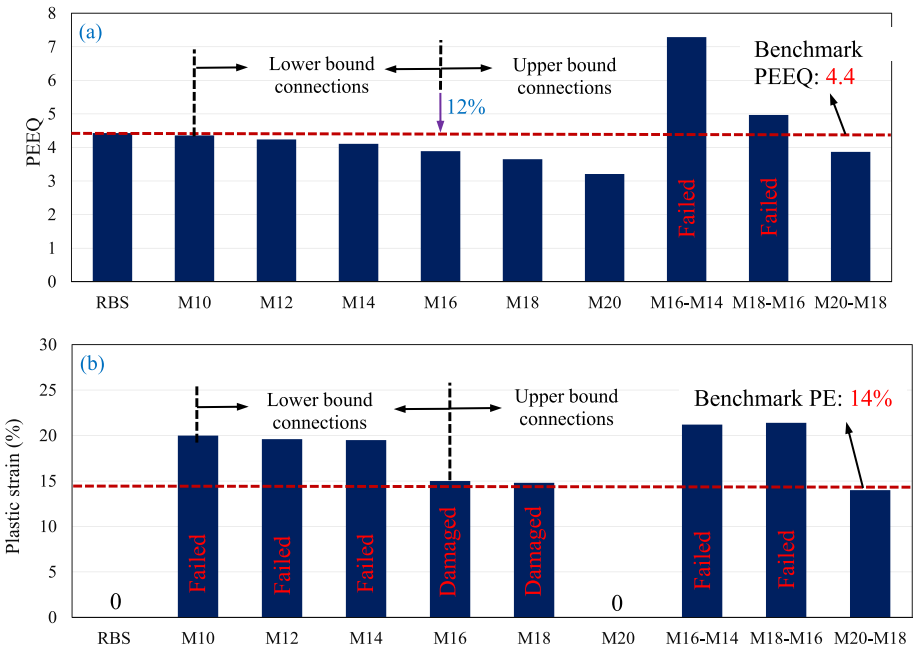

Fig. 15. Damage and failure modes of RBS and RBS-DNB connections: (a) PEEQ values at beam plastic hinge, and (b) plastic strain (PE) of bolts.

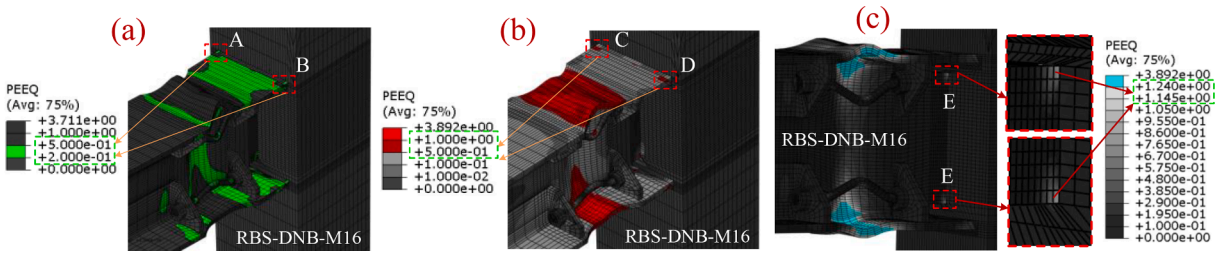

Fig. 16. Critical points of RBS and RBS-DNB connections: (a) CJP weld, (b) beam flange, and (c) shear tab.

M16 connections examined in this study. Note that connection RBS-M16 is deemed as representative of the rest of RBS-DNB connections, and therefore the observations presented here can be extended to the other RBS-DNB connections in this study. To define the beam ends' plastic hinge behavior, the normalized moment-story drift angle hysteresis curves of the RBS and RBS-DNB connections were first extracted from the Abaqus® results (Fig. 19(a) and (b), respectively). Based on these hysteresis curves, idealized skeleton curves of both connections were derived (red lines in Fig. 19(a) and (b)) and subsequently input into SAP2000® to define the behavior of the beam ends' plastic hinges.

7.3. Pushover results

Fig. 20(a)–(d) compare the pushover curves of the SMFs with RBS and RBS-M16 connections for the two pushover load patterns and two gravity load combinations. The results indicate that the RBS and RBS-M16 SMFs had the same elastic behavior. However, as expected, the SMF with RBS-M16 connections exhibited slightly higher lateral load capacity (around 5 % on average) than the one with RBS connections at ultimate roof displacement.

Fig. 21(a) and Fig. 21(b) show the distribution of plastic hinges in the SMFs with RBS and RBS-M16 connections at ultimate roof displacement. The results in Fig. 21(a) show that plastic hinge rotations of 0.05 to 0.08 rad developed at the first-floor beams in the SMF with RBS connections. The beam plastic hinge rotations of the RBS-M16 connections (Fig. 21 (b)) were between 0.03 and 0.08 rad. A similar behavior is observed at the second floor, where the beam plastic hinges of the RBS-M16 connections had generally smaller rotations than the reference RBS connections. Based on these results, it can be concluded that the SMF with RBS-DNB connections experience less overall damage than the SMF with RBS connections. It should be noted that whilst the difference between the lateral capacity of RBS and RBS-DNB systems is negligible, the latter is anticipated to exhibit better seismic performance when subjected to earthquake ground motions due to the lower rotation demands at the beams' plastic hinges.

Based on the results of this study, it can be concluded that RBS-DNB connections prove effective at increasing the flexural strength of the beam's reduced section and the energy dissipating capacity of the connection, as well as delaying damage to the beam's hinge. However, further research is necessary to examine: (i) different steel and material properties and cross sections, (ii) the relationship between the width of radii cuts and the bolts' diameter, and (iii) feasibility of using smaller bolt diameters to work as buckling restrained devices. Additional laboratory tests on actual RBS-DNB connections are also needed to fully validate the findings presented in this article.

8. Concluding remarks

This article investigated analytically the behavior of a new energy-dissipating RBS connection with Double Nut Bolts (RBS-DNB) and double shear tabs. The article also proposed a novel design method for such connections. A reference RBS connection from the literature was first modeled and calibrated in Abaqus® software. A set of RBS-DNB connections were then designed and modeled in Abaqus® to

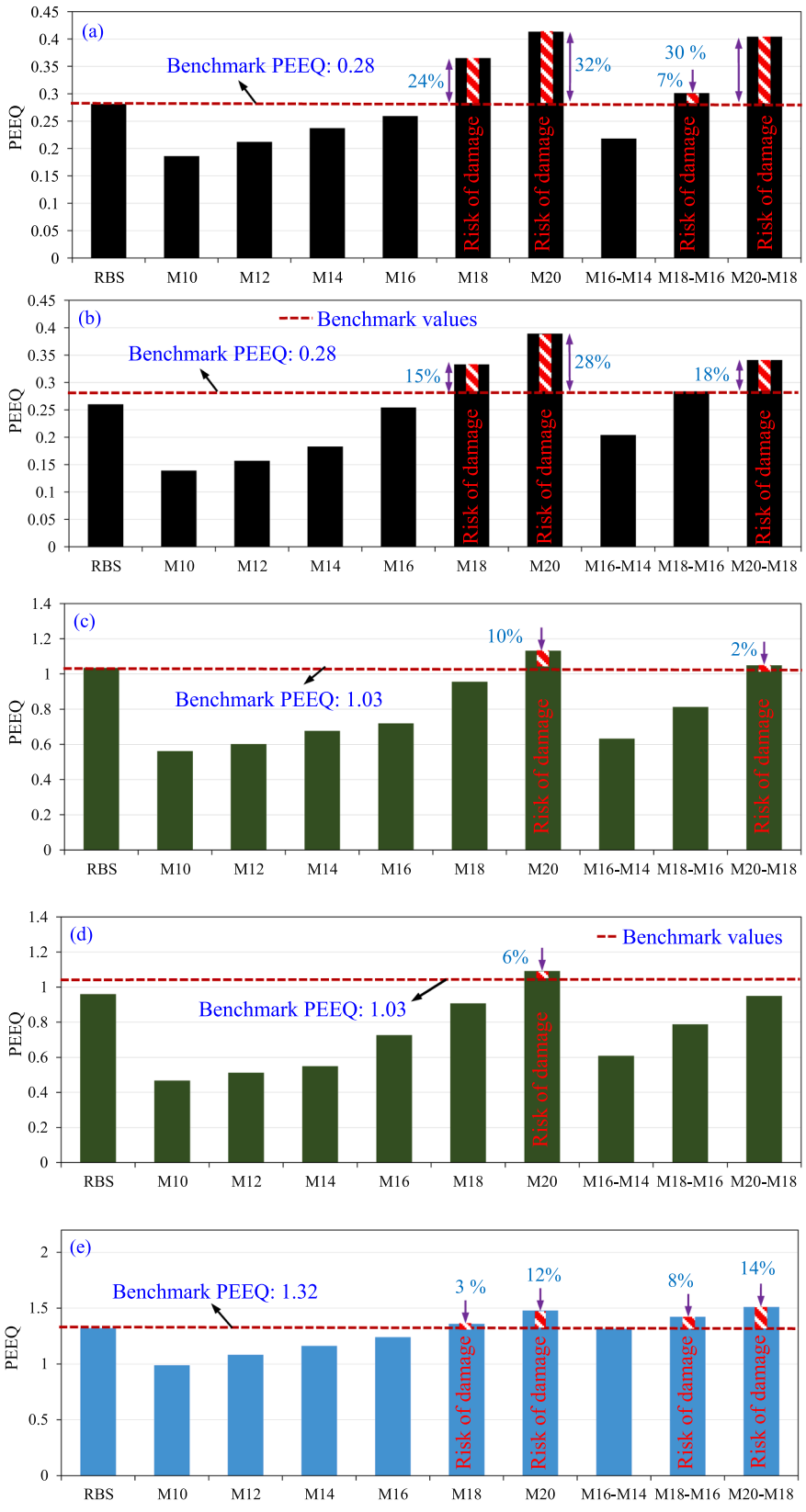

Fig. 17. Damage in beam flange and CJP weld of RBS and RBS-DNB connections at critical points: (a) CJP weld: point A, (b) CJP weld: point B, (c) beam flange: point C, (d) beam flange: point D, and (e) shear tab: point E.

Table 4
Potential damage and/or failure modes of RBS-DNB connections predicted by FE models.

ID	Potential damage	Failure
RBS [26]	–	–
RBS-M10	–	Bolts
RBS-M12	–	Bolts
RBS-M14	–	Bolts
RBS-M16	Bolts	–
RBS-M18	CJP welds 24 %↑, shear tabs 3 %↑	–
RBS-M20	Beam flange 10 %↑, CJP welds 32 %↑, shear tabs 12 %↑	–
RBS-M16-M14	–	Beam hinge, bolts
RBS-M18-M16	CJP welds 7 %↑, shear tabs 8 %↑	Beam hinge, bolts
RBS-M20-M18	Beam flange 2 %↑, CJP welds 30 %↑, shear tabs 14 %↑	–

investigate their cyclic response, beam strength, energy dissipation capacity, beam hinge deformation and initiation of hinging, and potential damage and failure modes. The numerical results from the RBS-DNB connections were then compared to those of the reference RBS connection. The seismic behavior of Special Moment Frames (SMFs) with either RBS or RBS-DNB connections was also examined using pushover analysis. Based on the results presented in this study, the following conclusions are drawn:

1. In all cases, RBS-DNB connections outperformed the reference RBS connection. Compared to the reference RBS connection, the main connection RBS-M16 had higher beam strength (~16.3 %) and more energy dissipation (~12 %), as well as lower beam hinge deformation (~28 %), and less beam hinge damage (~12 %). Also, the use of double nut bolts delayed beam hinge initiation in all RBS-DNB connections.
2. The damage assessment of the main RBS-M16 connection indicated that the double shear tabs increased the beam strength at column face zone due to the lower potential of damage to the beam flange, shear tab, and CJP weld of RBS-DNB connection. Also, the M16 bolts were severely damaged, as correctly predicted by the proposed RBS-DNB design method.
3. The results indicate that the use of over strength bolts in RBS-DNB connections resulted in potential damage and failure of other connection components (CJP welds, shear tabs, and beam flanges). Consequently, the new proposed design method successfully ensured the safe load-carrying mechanism of RBS-DNB connections. Moreover, the design method also predicted well the potential damage at the components of the connections.
4. The application of under strength bolts in RBS-DNB connections resulted in bolts failure due to weakness of the bolts. Therefore, the RBS-DNB design method is at an optimum level.
5. The use of different bolt sizes at the top and bottom of the beam led to premature failure of the beam hinge and high stress concentrations in the connection components. Accordingly, it is recommended to use bolts of the same sizes when designing RBS DNB connections. This in turn can also simplify the design and construction of RBS-DNB connections in actual SMF buildings.
6. Pushover analysis confirmed that SMFs with RBS-DNB connections had higher capacity (about 5 % for an SMF with RBS-M16 connections) and smaller rotations at the beam's plastic hinges compared to counterpart SMFs with RBS. Based on these results, it can be concluded that the SMF with RBS-DNB connections experience less damage than the SMF with RBS connections.

The experimental performance of RBS-DNB connections is currently

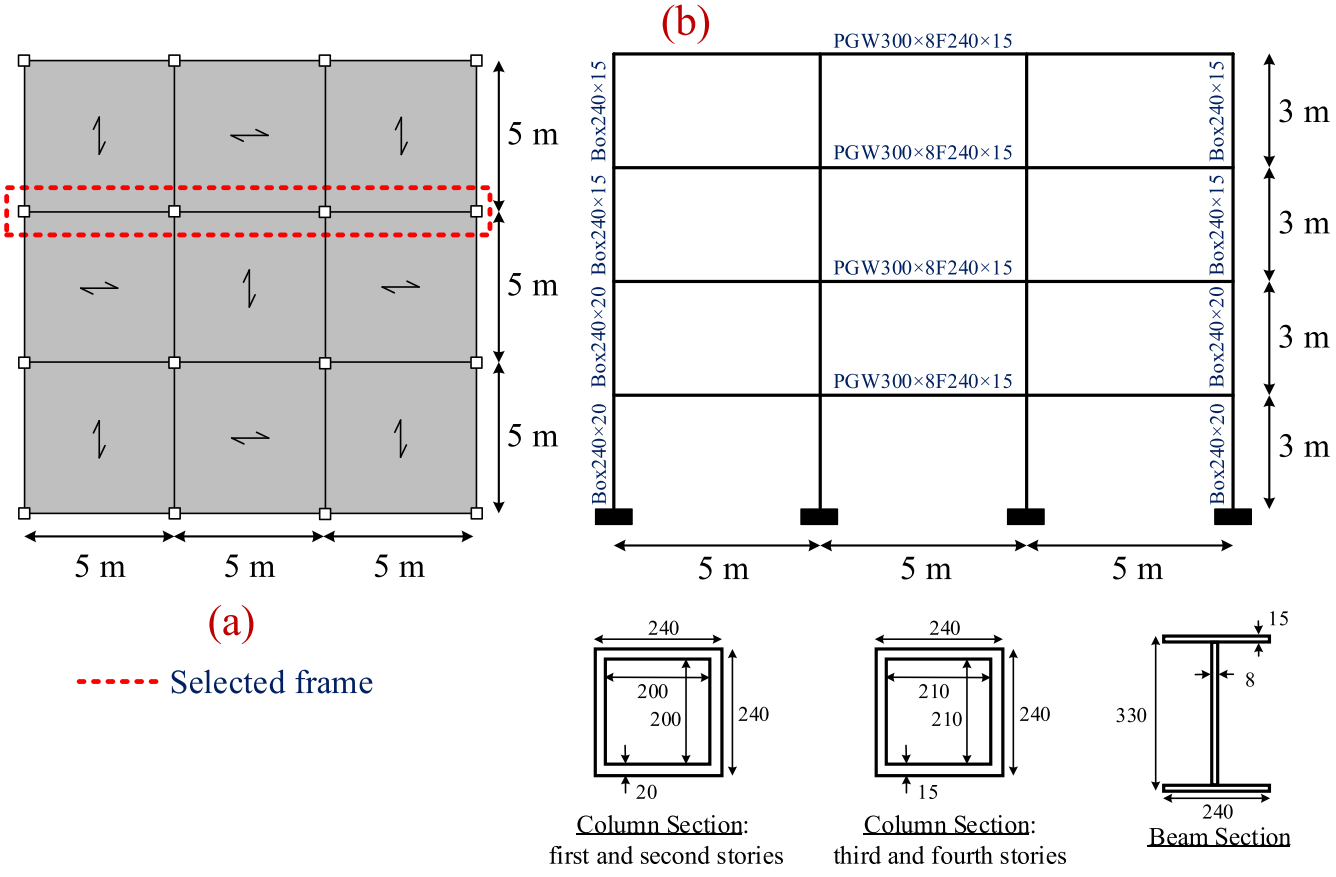

Fig. 18. SMF building: (a) plan view, and (b) elevation and box column and beam sections.

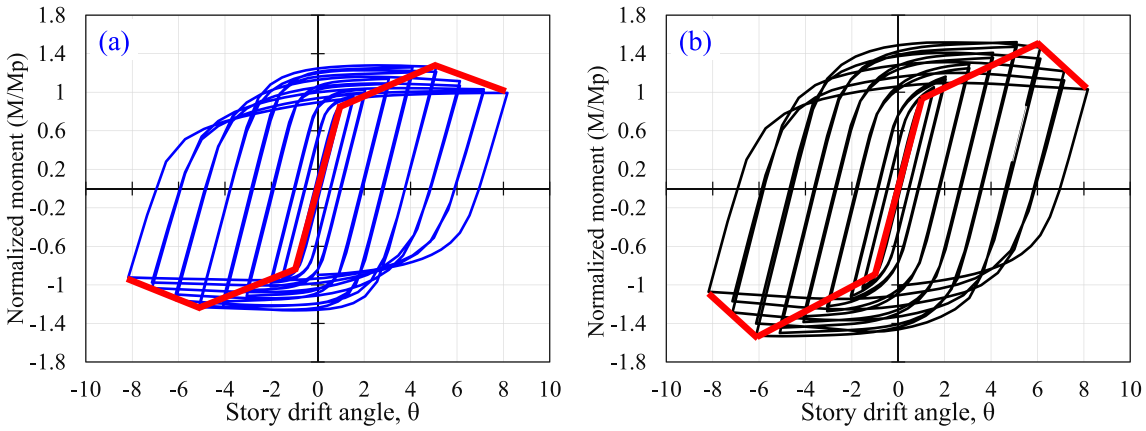

Fig. 19. Normalized moment-story drift angle curves from Abaqus® and skeleton curves of (a) RBS connection, and (b) RBS-M16 connection.

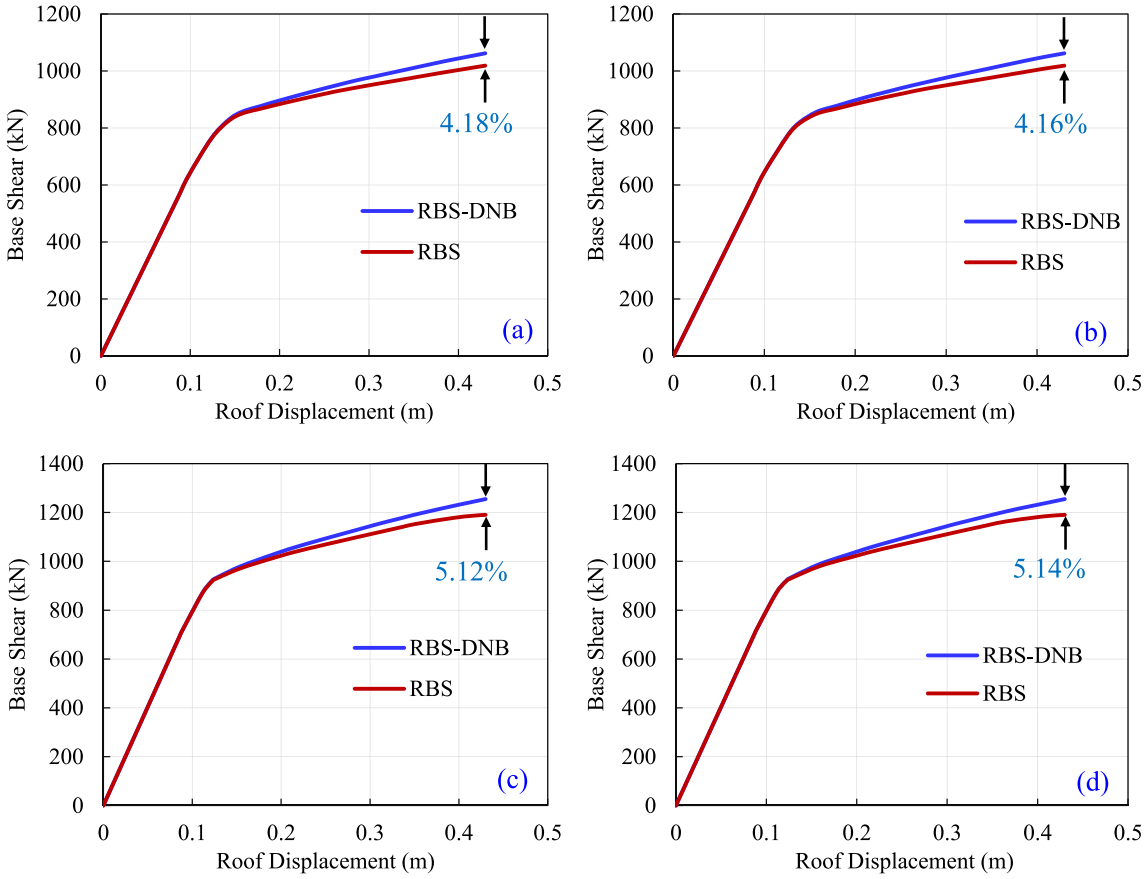

Fig. 20. Pushover curves of SMFs for different pushover load patterns and load cases: (a) first mode load pattern based on GH, (b) first mode load pattern based on GL, (c) uniform load pattern based on GH, and (d) uniform load pattern based on GL,

being investigated and the authors will publish the results in a forthcoming article.

CRediT authorship contribution statement

Bahram Mirzaie Abar: Formal analysis, Investigation, Conceptualization, Methodology, Software, Writing - original draft. **Yashar Bakhshayesh:** Formal analysis, Investigation, Methodology, Software, Conceptualization, Validation, Writing – original draft. **Reyes Garcia:** Investigation, Conceptualization, Visualization, Validation, Writing - review & editing. **Iman Hajirasouliha:** Conceptualization, Validation, Writing - review & editing.

Declaration of Competing Interest

The authors declare that they have no known competing financial interests or personal relationships that could have appeared to influence the work reported in this paper.

Data availability

No data was used for the research described in the article.

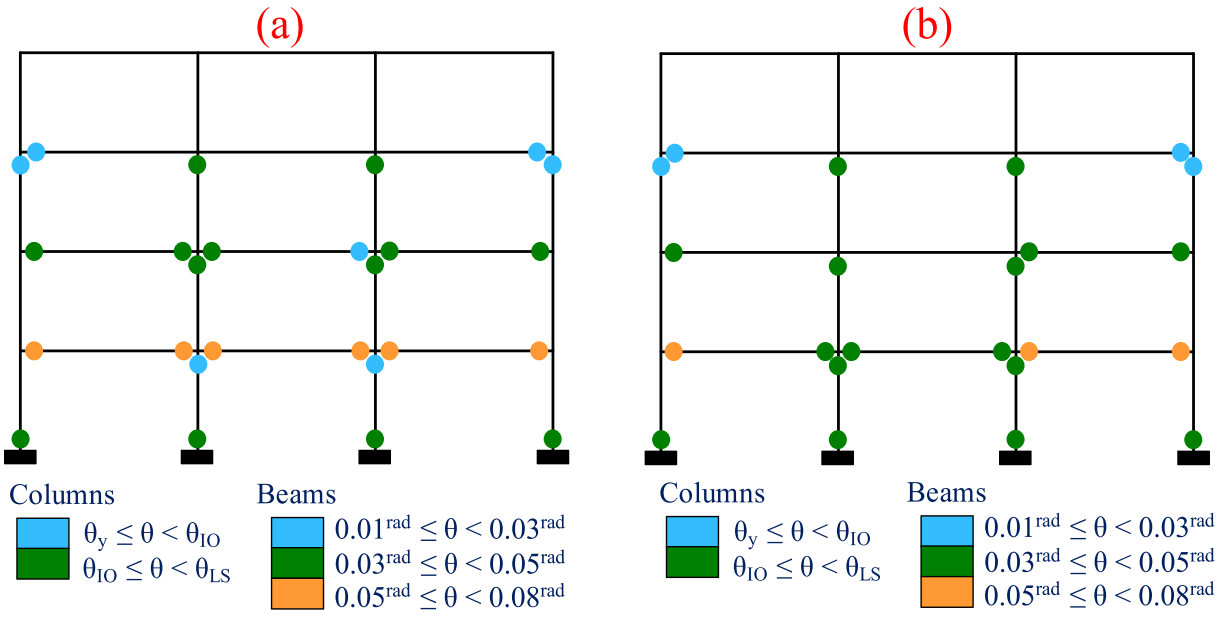

Fig. 21. Most critical distribution of the plastic hinges in (a) SMF with RBS connections, and (b) SMF with RBS-M16 connections.

Appendix A

Summary of RBS and RBS-DNB design calculation (connection RBS-M16).

Description	Calculations (units: N, mm)
Design calculation of the RBS connection [24] according to [12] (at section A–A) and the proposed method (at section C–C).	$C_{pr} = \frac{F_y + F_u}{2F_y} = \frac{261 + 397}{2 \times 261} = 1.26 > 1.2 \rightarrow C_{pr} = 1.2$ $Z_{RBS} = 2(b_{bf} - 2C)t_{bf}\left(\frac{d_b - t_{bf}}{2}\right) + \frac{t_{bw}}{4}(d_b - 2t_{bf})^2 + 2a_w{}^2\left(\frac{d_b - 2t_{bf} - a_w}{2}\right)$ $= 2 \times (240 - 2 \times 40) \times 15 \times \left(\frac{330 - 15}{2}\right) + \frac{8}{4}(330 - 2 \times 15)^2 + 2 \times 11^2 \times \left(\frac{330 - 2 \times 15 - 8}{2}\right) = 971136$ $M_{p,beam} = R_y F_{y,b} Z_{beam} = 1 \times 261 \times 1314000 = 342.95 \times 10^6$ $M_{p,RBS} = R_y F_{y,b} Z_{RBS} = 1 \times 261 \times 971136 = 253.46 \times 10^6$ $M_{pr} = C_{pr} R_y F_{y,b} Z_{RBS} = 1.2 \times 1 \times 261 \times 971136 = 304.16 \times 10^6$ $V_{pr} = \frac{2M_{pr}}{L_0 - (2a + b)} = \frac{2 \times 304.1 \times 10^6}{4700 - (2 \times 120 + 220)} = 143.4 \times 10^3$ $M_{u,D} = M_{ud,a} = M_{pr} + V_{pr} \times \left(a + \frac{b}{2}\right) = 304.1 \times 10^6 + 143.4 \times 10^3 \times (120 + 110) = 337.1 \times 10^6$ $M_{ud,c} = M_{ud,a} \times \frac{2L_{lb}}{L_0} = 337.11 \times 10^6 \times \frac{2 \times 2000}{4700} = 286.90 \times 10^6$ $Z_A = 2b_{bf}t_{bf}\left(\frac{d_b - t_{bf}}{2}\right) + \frac{t_{st}}{4}(d_b - 2t_{bf} - 2h_{a.c})^2 + \frac{t_{bw}}{4}(d_b - 2t_{bf} - 2h_{a.c})^2$ $= 2 \times 240 \times 15\left(\frac{330 - 15}{2}\right) + \frac{8}{4}(240 - 2 \times 15 - 2 \times 5)^2 + \frac{8}{4}(240 - 2 \times 15 - 2 \times 5)^2 = 1294000$ $Z_C = 2b_{bf}t_{bf}\left(\frac{d_b - t_{bf}}{2}\right) + \frac{t_{bw}}{4}(d_b - 2t_{bf})^2 = 2 \times 240 \times 15\left(\frac{330 - 15}{2}\right) + \frac{8}{4}(330 - 2 \times 15)^2 = 1314000$ $M_A = \varphi_d Z_A R_{y,b} F_{y,b} = 1 \times 1294000 \times 261 = 337.73 \times 10^6$ $M_C = \varphi_n Z_C R_y F_y = 0.9 \times 1314000 \times 261 = 308.65 \times 10^6$ $\frac{M_{ud,a}}{M_A} = \frac{337.1 \times 10^6}{337.73 \times 10^6} = 0.99.$ Likewise, $\frac{M_{ud,c}}{M_C} = \frac{286.90 \times 10^6}{308.65 \times 10^6} = 0.93$
Step 1: Assume the initial diameter of the bolts (d_{cb}).	According to the recommendations presented in Section 2 at Step 1, the diameter of the bolts was considered as 16 mm (M16).

(*continued on next page*)

(*continued*)

Description	Calculations (units: N, mm)
Step 2: Calculate (F_{nb}) according to Eqs. (1), 2 (a) to 2(e).	$F_{n,b} = \varphi_c F_{cr} A_{tb} = 0.9 \times 212.41 \times 201.05 = 38.43 \times 10^3$ If $\frac{F_{y,bolt}}{F_e} = \frac{900}{242.2} = 3.716 > 2.25 \rightarrow F_{cr} = 0.877 F_e = 0.877 \times 242.2 = 212.41$ $F_e = \frac{\pi^2 E}{\left(\frac{L_c}{r}\right)^2} = \frac{\pi^2 \times 210 \times 10^3}{\left(\frac{117}{4}\right)^2} = \frac{9.87 \times 210 \times 10^3}{855.56} = 242.2 L_c = 0.65 \times L_{tb} = 0.65 \times 180 = 117$. Likewise, $r = \frac{d_{tb}}{4} = \frac{16}{4} = 4$
Step 3: Calculate ($M_{ud,a}$) according to Eqs. (3) to (5).	$M_{p,b} = R_y F_{y,b} Z_{RBS} + 4 F_{n,b} h_b = 253.46 \times 10^6 + 4 \times 38.43 \times 10^3 \times (110) = 270.37 \times 10^6$ $M_{pr,b} = C_{pr} R_y F_{y,b} Z_{RBS} + 4 F_{n,b} h_b = 304.1 \times 10^6 + 4 \times 38.43 \times 10^3 \times (110) = 321.09 \times 10^6$ $V_{pr,b} = \frac{2 M_{pr,b}}{L_0 - (2a + b)} = \frac{2 \times 321.09 \times 10^6}{4700 - (2 \times 120 + 220)} = 151.45 \times 10^3 M_{ud,a} = M_{pr,b} + V_{pr,b} \times \left(a + \frac{b}{2}\right) = 321.09 \times 10^6 + 151.45 \times 10^3 \times (120 + 110) = 355.92 \times 10^6$
Step 4: Calculate ($M_{ud,c}$) according to Eq. (6).	$M_{ud,c} = M_{ud,a} \times \frac{2 L_{lb}}{L_0} = 355.92 \times 10^6 \times \frac{2 \times 2000}{4700} = 302.91 \times 10^6$
Step 5: Calculate (M_A) and (M_C) according to Eqs. (7) to (10).	$M_A = \varphi_d Z_A R_{y,b} F_{y,b} = 1 \times 1409560 \times 261 = 367.9 \times 10^6$ $M_C = \varphi_n Z_C R_y F_y = 0.9 \times 1314000 \times 261 = 308.65 \times 10^6$ $Z_A = 2 b_{bf} t_{bf} \left(\frac{d_b - t_{bf}}{2}\right) + \frac{t_{st}}{2}(d_b - 2t_{bf} - 2h_{a,c})^2 + \frac{t_{bw}}{4}(d_b - 2t_{bf} - 2h_{a,c})^2$ $= 2 \times 240 \times 15 \left(\frac{330 - 15}{2}\right) + \frac{16}{2}(240 - 2 \times 15 - 2 \times 22)^2 + \frac{8}{4}(240 - 2 \times 15 - 2 \times 22)^2$ $= 1409560 Z_C = 2 b_{bf} t_{bf} \left(\frac{d_b - t_{bf}}{2}\right) + \frac{t_{bw}}{4}(d_b - 2t_{bf})^2 = 2 \times 240 \times 15 \left(\frac{330 - 15}{2}\right) + \frac{8}{4}(330 - 2 \times 15)^2 = 1314000$
Step 6: Control the beam moment capacities according to Eqs. (11) and (12).	$M_{ud,a} \le M_A = 355.92 \times 10^6 \approx 353.51 \times 10^6$ *O.K.* $\rightarrow \frac{M_{ud,a}}{M_A} = \frac{355.92 \times 10^6}{353.51 \times 10^6} = 1.00$ *OK* $M_{ud,c} \le M_C = 302.91 \times 10^6 < 308.6 \times 10^6 \rightarrow$ *OK* $\rightarrow \frac{M_{ud,c}}{M_C} = \frac{302.91 \times 10^6}{308.6 \times 10^6} = 0.98$ *OK*
Comparison step: flexural strengths of RBS connection, beam, and RBS-DNB connection	**Beam** (calculated before Step 1):$M_{p,beam} = 342.95 \times 10^6$ **RBS** (calculated before Step 1):$M_{p,RBS} = 253.46 \times 10^6$ **RBS-DNB** (calculated in Step 3):$M_{p,b} = 270.37 \times 10^6$ Flexural strength recovered by the double nut bolts (%):$\frac{M_{p,b} - M_{p,RBS}}{M_{p,beam} - M_{p,RBS}} = \frac{270.37 \times 10^6 - 253.46 \times 10^6}{342.95 \times 10^6 - 253.46 \times 10^6} = 18.9\%$ Therefore the M16 bolts recovered ~ 18.9% of the RBS flexural strength.

References

[1] Wang S, Lai JW, Schoettler MJ, Mahin SA. Seismic assessment of existing tall buildings: A case study of a 35-story steel building with pre-Northridge connection. Eng Struct 2017;141:624–33.

[2] Adan SM, Gibb W. Experimental evaluation of kaiser bolted bracket steel moment-resisting connections. Eng J-Am Instit Steel Constr INC 2009;46(3):181–95.

[3] Pryor SE, Murray TM. Next generation partial strength steel moment frames for seismic resistance. Research, Development, and Practice in Structural Engineering and Construction. In: Vimonsatit V, Singh A, Yazdani S, editors. Proceedings of the First Australasia and South-East Asia Structural Engineering and Construction Conference; 2013. p. 27–32.

[4] Abar BM, Ghobadi MS. Double shear bolted bracket moment connections, part 1: Four-bolt configuration design methodology. J Constr Steel Res 2020;174:106280.

[5] Sato A, Newell JD, Uang CM. Cyclic behaviour and seismic design of bolted flange plate steel moment connections. Eng J 2008;45(4):221.

[6] Ghobadi MS, Mirzaie Abar B. Development of new fully restrained bolted bracket moment connections for strong joints. Arch Civil Mech Eng 2021;21(4):1–30.

[7] Hantouche EG, Rassati GA, Kukreti AR, Swanson JA. Built-up T-stub connections for moment resisting frames: Experimental and finite element investigation for prequalification. Eng Struct 2012;43:139–48.

[8] Sumner III EA. Unified design of extended end-plate moment connections subject to cyclic loading. Blacksburg, Virginia: College of Engineering, Virginia Polytechnic, Institute and State University; 2003. Doctoral thesis.

[9] Abar BM, Ghobadi MS. New generation of bolted bracket connections: Safe load-carrying capacity and structural damage assessment. Eng Struct 2022;252:113662.

[10] Tartaglia R, D'Aniello M, Rassati GA, Swanson JA, Landolfo R. Full strength extended stiffened end-plate joints: AISC vs recent European design criteria. Eng Struct 2018;159:155–71.

[11] Hosseini SM, Rahnavard R. Numerical study of steel rigid collar connection affecting cyclic loading. Eng Struct 2020;208:110314.

[12] ANSI/AISC 358s2-20. Prequalified Connections for Special and Intermediate Steel Moment Frames for Seismic Applications. Chicago, Illinois, USA: American Institute of Steel Construction (AISC).

[13] Horton TA, Hajirasouliha I, Davison B, Ozdemir Z. More efficient design of reduced beam sections (RBS) for maximum seismic performance. J Constr Steel Res 2021;183:106728.

[14] Horton TA, Hajirasouliha I, Davison B, Ozdemir Z, Abuzayed I. Development of more accurate cyclic hysteretic models to represent RBS connections. Eng Struct 2021;245:112899.

[15] Pachoumis DT, Galoussis EG, Kalfas CN, Efthimiou IZ. Cyclic performance of steel moment-resisting connections with reduced beam sections—experimental analysis and finite element model simulation. Eng Struct 2010;32(9):2683–92.

[16] Zhang X, Ricles JM. Experimental evaluation of reduced beam section connections to deep columns. J Struct Eng 2006;132(3):346–57.

[17] Horton TA, Hajirasouliha I, Davison B, Ozdemir Z. Accurate prediction of cyclic hysteresis behaviour of RBS connections using deep learning neural networks. Eng Struct 2021;247:113156.

[18] Chen C, Qiao H, Wang J, Chen Y. Progressive collapse behaviour of joints in steel moment frames involving reduced beam section. Eng Struct 2020;225:111297.

[19] Plumier A. The dogbone: back to the future. Eng J-Am Instit Steel Constr 1997;34:61–7.

[20] Tsavdaridis KD, Papadopoulos T. A FE parametric study of RWS beam-to-column bolted connections with cellular beams. J Constr Steel Res 2016;116:92–113.

[21] Atashzaban A, Hajirasouliha I, Jazany RA, Izadinia M. Optimum drilled flange moment resisting connections for seismic regions. J Constr Steel Res 2015;112:325–38.

[22] Liu C, Wu J, Xie L. Seismic performance of buckling-restrained reduced beam section connection for steel frames. J Constr Steel Res 2021;181:106622.

[23] Sofias CE, Kalfas CN, Pachoumis DT. Experimental and FEM analysis of reduced beam section moment endplate connections under cyclic loading. Eng Struct 2014;59:320–9.

[24] ANSI/AISC 360-16. Specification for Structural Steel Buildings. Chicago, Illinois, USA: American Institute of Steel Construction (AISC). 2016.

[25] ANSI/AISC 341-16. Seismic Provisions for Structural Steel Buildings. Chicago, Illinois, USA: American Institute of Steel Construction (AISC); 2016.
[26] Ghassemieh M, Mirghaderi SR. Cyclic dependency assessment of RBS moment connection in box-column. J Constr Steel Res 2021;177:106472.
[27] Abaqus FEA. Analysis User's Manual 6.14. Providence, RI: Dassault Systemes Simulia Corp.; 2011.
[28] Bakhshayesh Y, Shayanfar M, Ghamari A. Improving the performance of concentrically braced frame utilizing an innovative shear damper. J Constr Steel Res 2021;182:106672.
[29] Chisari C, Francavilla AB, Latour M, Piluso V, Rizzano G, Amadio C. Critical issues in parameter calibration of cyclic models for steel members. Eng Struct 2017;132:23–138.
[30] Abar BM, Ghobadi MS, Jazany RA. Double shear bolted bracket moment connections, part 2: Four-bolt configuration response evaluation. J Constr Steel Res 2020;174:106281.
[31] RHUDRC 2014. 2800-Standard for Design of Structures against Earthquakes, 4th ed., Road, Housing and Urban Development Research Center, Teheran, Iran.
[32] ASCE. ASCE/SEI 41-06 - Seismic rehabilitation of existing buildings. Reston, VA, USA: American Society of Civil Engineers; 2007.
[33] CSI. Analysis reference manual for SAP2000, Etabs, Safe and CSIBridge. Berkeley, CA, USA: Computers and Structures, Inc.; 2015.